Marine Geology 443 (2022) 106653

Contents lists available at ScienceDirect

Marine Geology

journal homepage: www.elsevier.com/locate/margo

Research Paper

Oceanic passage of hurricanes across Cay Sal Bank in The Bahamas over the last 530 years

Tyler S. Winkler [a,c,*], Peter J. van Hengstum [a,b], Jeffrey P. Donnelly [c], Elizabeth J. Wallace [d], Nicole D'Entremont [c], Andrea D. Hawkes [e], Christopher V. Maio [f], Richard M. Sullivan [a], Jonathan D. Woodruff [g]

[a] Department of Oceanography, Texas A&M University, College Station, TX 77843, USA
[b] Department of Marine and Coastal Environmental Science, Texas A&M University at Galveston, Galveston, TX 77554, USA
[c] Department of Geology and Geophysics, Woods Hole Oceanographic Institution, Woods Hole, MA 02543, USA
[d] Massachusetts Institute of Technology/Woods Hole Oceanographic Institution Joint Program in Oceanography, Woods Hole, MA 02543, USA
[e] Department of Earth and Ocean Sciences, University of North Carolina Wilmington, Wilmington, NC 28403, USA
[f] Department of Geosciences, University of Alaska Fairbanks, Fairbanks, AK 99775, USA
[g] Department of Geosciences, University of Massachusetts, Amherst, MA 01003, USA

ARTICLE INFO

Editor: Prof Edward Anthony

Keywords:
Hurricanes
Sedimentology
Natural hazards
Paleoclimate
Paleoceanography
Other carbonate shelves and processes
N Atlantic
Bahamas
Florida straits

ABSTRACT

Islands across the Bahamian Archipelago have been devastated by five major hurricanes from 2010 to 2020 CE, including Category 5 Hurricane Dorian in 2019 that inundated parts of Abaco and Grand Bahama with up to 4 m of surge, killing 84 people and leaving >245 others missing. Up to 1 m relative sea-level rise is estimated for The Bahamas by 2100 CE, which could enhance flooding from weaker storms (<Category 3) in low-lying coastal areas. Problematically, Bahamian hurricane activity is highly spatially-heterogenous over the last 170 years, meaning that long-term regional hurricane frequency remains poorly constrained, especially for weaker Category 1–2 events that are less-likely to be detected by most sediment-based paleo-hurricane reconstructions. We present a 530-year record of hurricane passage from Hine's Blue Hole on Cay Sal Bank, The Bahamas. Hine's Hole has an accumulation rate of 2–3.2 cm/yr, making it among the highest-resolution hurricane reconstructions to date. Unlike many paleo-hurricane reconstruction sites, Hine's Hole is not surrounded by coastal landmasses that can dampen currents and waves produced by hurricanes, so it archives most ≥Category 1 hurricanes passing within 115 km during the 170-year instrumental record (1850 CE-present) and may also document intense tropical or winter storms. Hine's Hole archives ~16 intense storms per century from 1850 to 2016 CE, but documents three periods from 1505 to 1530 CE, 1570 to 1620 CE, and ~ 1710 to 1875 CE with over twice as many intense storms per century. These active periods correspond to other high-resolution reconstructions from the Bahamian Archipelago and Florida Keys, but the magnitude of the increase is much higher given that Hine's Hole archives evidence of weaker and more distal storms. As such, this reconstruction provides unprecedented insight into changes in hurricane activity within the pre-industrial climate system and demonstrates that recurrence intervals based on the 170-year instrumental record can severely underestimate the threat hurricanes pose certain localities.

1. Introduction

The year 2020 Common Era (CE) observed the highest number of named Atlantic tropical cyclones (30) since the instrumental record began in 1850 CE. From 1980 to 2020 CE, 52 tropical cyclones have individually caused ≥$1 billion USD in damage (adjusting for inflation), collectively resulting in $997.3 billion USD in damages (Consumer Price Index adjusted) and 6593 verified deaths in the United States alone (Smith, 2020). Growing coastal populations and development will continue to increase the vulnerability of coastal communities to deleterious impacts of extreme flooding events like tropical cyclones (Pielke Jr. et al., 2008; Woodruff et al., 2013), and Davenport et al. (2021) propose that anthropogenically facilitated climate change is directly responsible for a substantial portion of these flood related damages.

* Corresponding author at: Department of Geology and Geophysics, Woods Hole Oceanographic Institution, Woods Hole, MA 02543, USA.
E-mail address: twinkler@whoi.edu (T.S. Winkler).

https://doi.org/10.1016/j.margeo.2021.106653
Received 6 May 2021; Received in revised form 21 September 2021; Accepted 22 September 2021
Available online 1 October 2021

Projected warming of the planet by 2 °C during the 21st century may cause: i. an increase in the global proportion of intense tropical cyclones (Emanuel et al., 2008; Emanuel, 2013; Knutson et al., 2020; Korty et al., 2017; Sobel et al., 2016; Walsh et al., 2015; Walsh et al., 2016); ii. an increase in the amount of precipitation delivered by tropical cyclones (Patricola and Wehner, 2018), iii. an increase in tropical cyclone size and rainfall area (Chavas et al., 2016; Lin et al., 2015); and iv) reduced tropical cyclone translational speed that can enhance landscape flooding from surge and rainfall (Kossin, 2018). Coupled with high-confidence projections of an additional ~1 m global sea level-rise by 2100 CE (Oppenheimer and Hinkel, 2019), coastal populations are becoming increasingly threatened by tropical cyclone storm surge amplification, winds, and flooding (Miller et al., 2013; Pielke Jr. et al., 2008; Vacchi et al., 2018; Wong et al., 2014; Woodruff et al., 2013).

Future tropical cyclone risk assessments mostly rely on the tropical cyclone instrumental record over the last 170 years (International Best Track Archive for Climate Stewardship-IBTrACS; (Knapp et al., 2018; Knapp et al., 2010). The regional frequency of Atlantic tropical cyclones, referred to hereafter as hurricanes, is spatially-heterogenous throughout the Atlantic since 1850 CE, and significant variability in >Category 2 hurricane frequency can be observed at islands less than 300 km apart in the Bahamian Archipelago (Winkler et al., 2020). Problematically, the relatively short-temporal scale of the instrumental record makes it unclear if observed spatial heterogeneity of Atlantic hurricane frequency (see Fig. 1 in Winkler et al., 2020) persists on longer timescales (i.e., centennial and millennial; (Donnelly et al., 2015; Landsea et al., 2006). Knowledge of Atlantic hurricane activity can be extended using historical accounts, but these records are incomplete and biased toward well populated regions with preserved recorded histories (Chenoweth and Divine, 2008; Trouet et al., 2016). Many lower resolution sedimentary and geochemical records of paleo-hurricane impacts have helped extend the record of Atlantic storms back thousands of years (Biguenet et al., 2021; Bregy et al., 2018; Donnelly and Woodruff, 2007; Liu and Fearn, 1993; Liu and Fearn, 2000; Mallinson et al., 2011; Oliva et al., 2018; van Hengstum et al., 2016; Yang et al., 2020). However, these records tend to have higher age-uncertainties and typically archive only the most intense hurricane events. Further, significant spatial and temporal gaps remain in the coverage of existing records, thus limiting confidence in interpreting changes in hurricane climatology on centennial timescales.

Over the last 10 years, an array of near-annually resolved sedimentary archives from deep coastal basins have expanded temporal understanding of regional hurricane variability throughout the North Atlantic, revealing significant variations in landfall frequency at centennial and multi-decadal scales (Brandon et al., 2013; Denomee et al., 2014; Donnelly et al., 2015; Lane et al., 2011; Schmitt et al., 2020; Wallace et al., 2019; Wallace et al., 2021b; Wallace et al., 2021c; Winkler et al., 2020). These studies also reveal substantial spatial heterogeneity in hurricane activity throughout the last 2000 years, meaning that variability recorded by a single site may not necessarily reflect changing climatology throughout the entire Atlantic. Based on an assessment of downscaled hurricane model runs spanning the last millennium, Wallace et al. (2021a) suggest that much of the century-scale hurricane frequency variability in individual paleo-hurricane records from The Bahamas may be related to local-scale weather patterns rather than broader regional climate forcing. However, as more near-annually resolved studies emerge from the Bahamian Archipelago, synchronous periods of active/quiet hurricane activity persist through multiple records, and a statistical compilation of these records by Wallace et al. (2021c) that smooths out local-scale variations in storm frequency reveals robust centennial scale patterns (see Wallace et al. (2021b) for updated compilation). Thus, a climate mediated signal may be emerging from the compiled regional hurricane reconstructions, but the global and regional climatic mechanisms and their relative influence remain an active area of study.

Here we present a 530 year, near annually-resolved sedimentary record from a subtidal, oceanic blue hole on Cay Sal Bank, The Bahamas. To date, this record is one of the highest resolution sedimentary reconstructions of paleo-hurricane activity from the North Atlantic Ocean owing to the high sedimentation rate in the site. This site is not sheltered from wave action by supratidal geomorphology, meaning that coarse-sediment storm deposits archived in the stratigraphy may be derived from weaker storms like ≥Category 1 hurricanes (Saffir-Simpson Scale) that pass within a large radius of the blue hole, or even more proximal tropical storms or winter storms that can produce locally intense waves

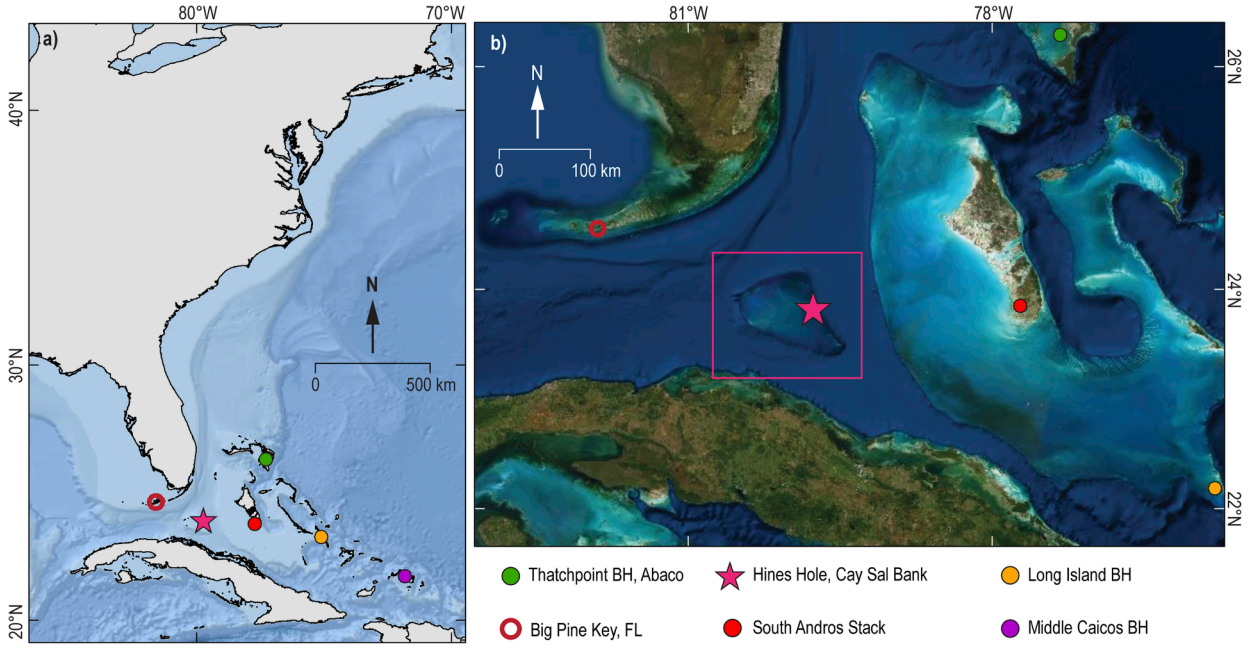

Fig. 1. a) Location of Cay Sal Bank, The Bahamas in the northern Atlantic (pink star) as well as the location of high-resolution hurricane reconstructions from the Bahamian Archipelago (colored circles correspond to reconstructions in Figs. 8 and 9), the northeastern US (green squares), and Gulf of Mexico (red squares; basemap source: *Esri Oceans*). b) Visible spectrum (true-colour) satellite imagery from ESRI of Cay Sal Bank (pink box), which is emplaced between south Florida and Cuba in the center of the Florida Straits. (For interpretation of the references to colour in this figure legend, the reader is referred to the web version of this article.)

and currents. This is in contrast to previous locations where paleo-hurricane records have been developed that only record more proximal intense hurricane strikes (≥Category 2) (e.g., Bregy et al., 2018; Lane et al., 2011; van Hengstum et al., 2016; Wallace et al., 2019; Wallace et al., 2021c; Winkler et al., 2020). This single record captures spatiotemporal trends in storminess that emerge from a compilation of existing highly-resolved records of Bahamian hurricane activity (Wallace et al., 2021b; Wallace et al., 2021c).

2. Regional setting: Hine's Hole on Cay Sal Bank

Hine's Hole is located on the eastern margin of Cay Sal Bank, The Bahamas (Figs. 1, 2), so named after pioneering surveying efforts led by Dr. Albert Hine (Hine and Steinmetz, 1984). This slightly oblong blue hole is 340 m wide north to south, and 315 m wide east to west, with a gently sloping bathymetry from 80 to 95 m below sea level (mbsl). The 6000 square km Cay Sal Bank is the westernmost carbonate platform in the Bahamian Archipelago, and is considered partially drowned with an average bank-top depth of ~10 mbsl (Hine and Steinmetz, 1984; Purkis et al., 2014). Cay Sal Bank's elevation is lower relative to other platforms in the Bahamian Archipelago, including the Little Bahama Bank and the Great Bahama Bank, and both of which have well developed platform-edge reefs. As such, the growth rate of platform-edge reefs along Cay Sal Bank was outpaced by rapid relative sea-level rise that peaked during the mid-Holocene (Hine and Steinmetz, 1984), making Cay Sal Bank one of just two Bahamian platforms with non-aggraded margins (Purkis et al., 2014).

Cay Sal Bank has limited biologic productivity at both a micro- and macro-scale, which limits biogenic carbonate sediment production (Goldberg, 1983; Purkis et al., 2014), and inorganic carbonate mud produced in the water column is winnowed-off the bank-top by strong currents and waves (Purkis et al., 2014). As such, average sediment

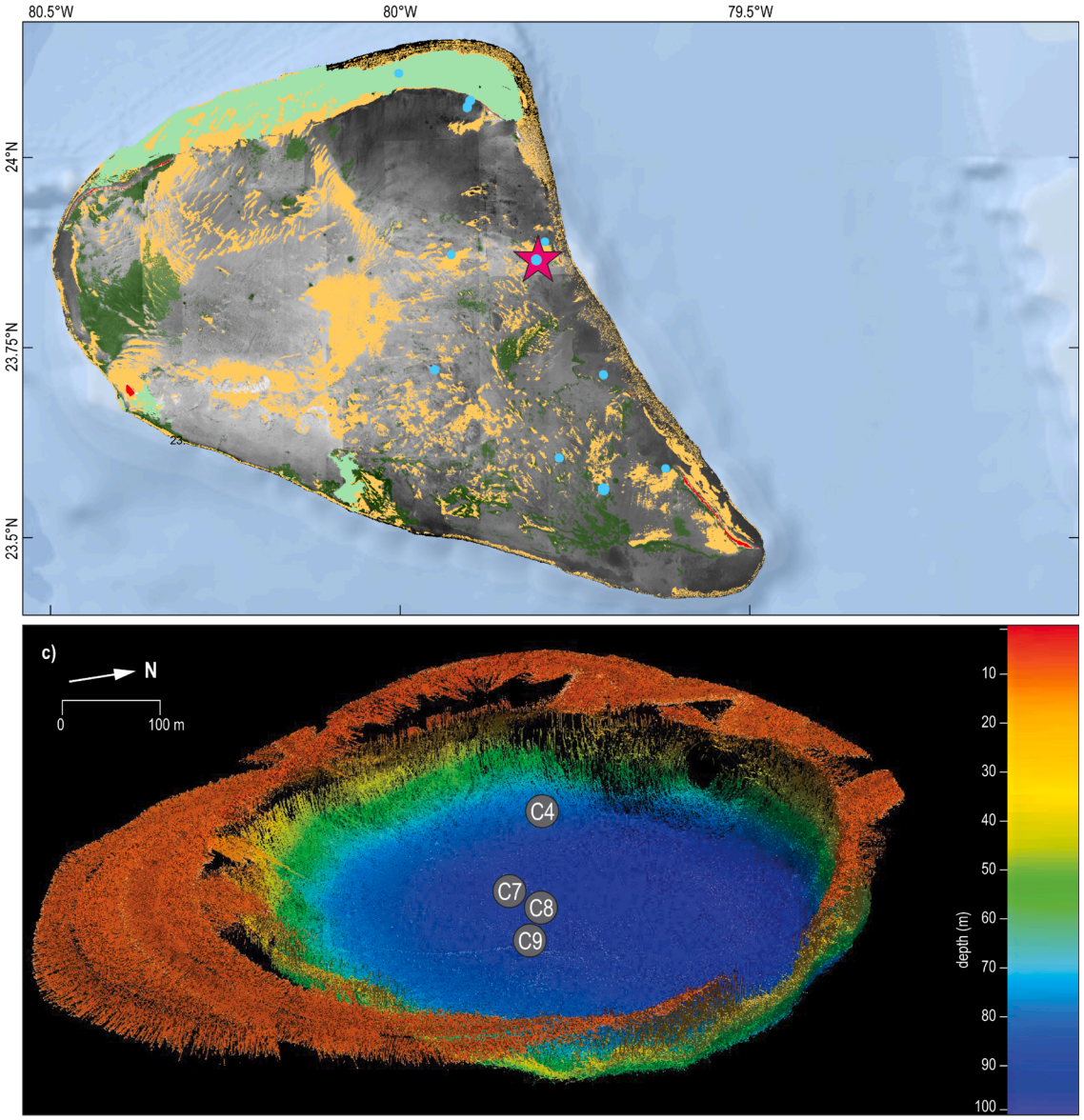

Fig. 2. a) Location of Hine's Hole (pink star) on the northeastern flank of Cay Sal Bank, The Bahamas (basemap source: *Esri Oceans*). This map shows high resolution bathymetry (lighter = shallower, darker = deeper) as well as the location of large sand accumulations (dotted tan and light green areas) and habitat features on Cay Sal Bank. The bathymetric and habitat data is used courtesy of the Khaled Bin Sultan Living Oceans Foundation, and the collection methods and further discussion of the data can be found in (Purkis et al., 2014). b) Aerial photograph of Hine's Hole. c) 3D multibeam bathymetry of Hine's Hole with coring locations noted by grey circles. This survey was completed for this study onboard the MV Alucia in April 2016 using a Teledyne Reson SeaBat 7160 Multibeam Echo Sounder, and proprietary Teledyne PDS software was used to produce the image. (For interpretation of the references to colour in this figure legend, the reader is referred to the web version of this article.)

cover on Cay Sal Bank is generally less than 10 cm (Goldberg, 1983). In comparison, the Holocene sediment cover on the Little Bahama Bank is 2 m (Rasmussen et al., 1990) and is up to ~5 m thick in some areas of Bermuda (Ashmore and Leatherman, 1984). Previous work by Hine and Steinmetz (1984) and Purkis et al. (2014) document scattered and thin (<2 m) deposits of sand-sized particles made up of intraclasts, peloids, and skeletal grains on the windward (eastern) portion, and carbonate gravels on the leeward (western and central) region (Fig. 2a). Sand samples contain less than 30% identifiable skeletal grains, and sand particles are mostly benthic foraminifera, echinoderms, corals, bryozoa, arthropods, and coralline algae (the remaining 70% are unidentifiable weathered grains). While bank-top sediment accumulation is scarce, geophysical surveys by Hine and Steinmetz (1984) documented thick sediment accumulation in Hine's Hole.

Since 1975 CE, seasonally-averaged winds reveal that the easterly trade winds dominate the surface field across Cay Sal Bank throughout

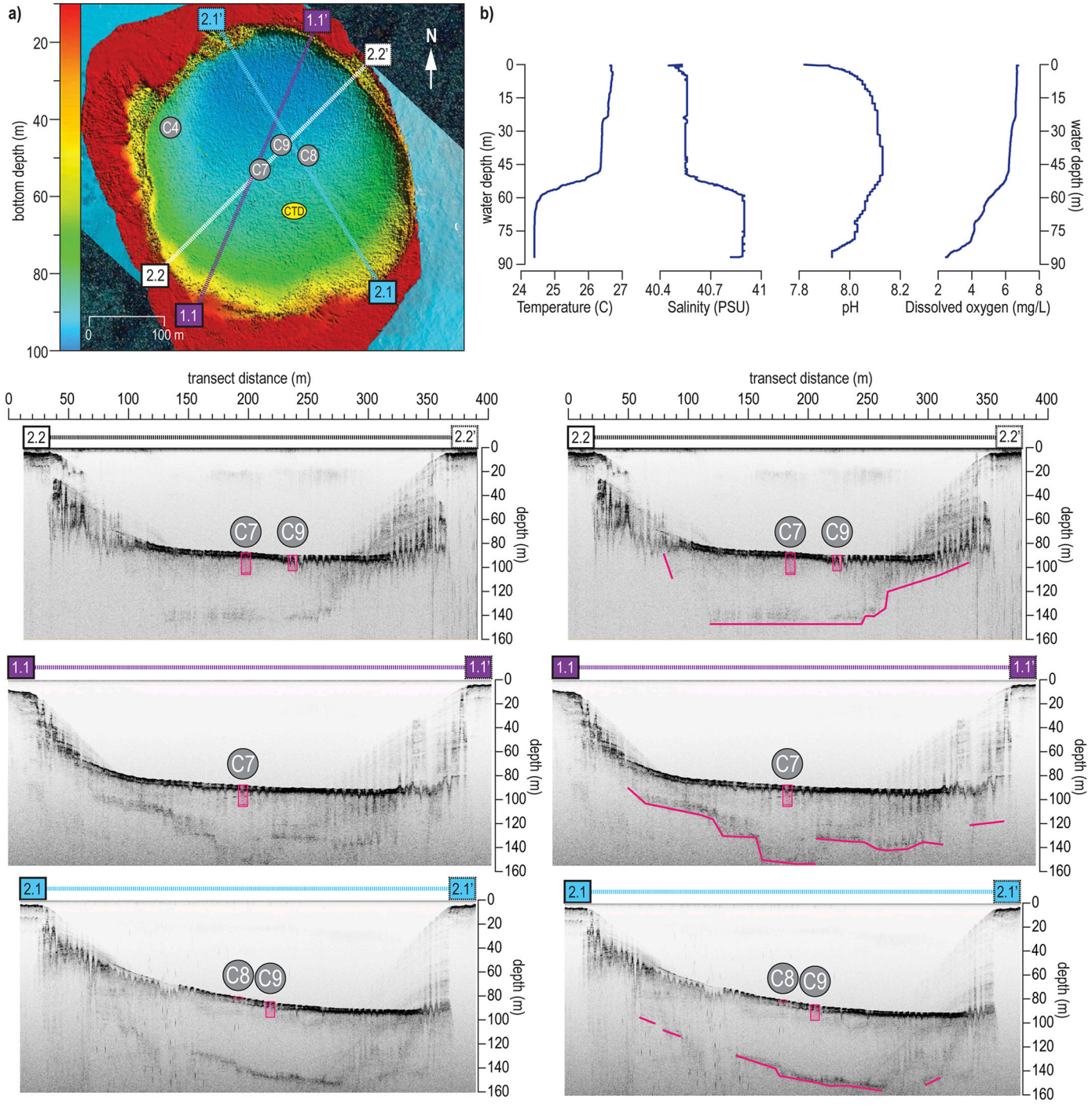

Fig. 3. a) 2D depiction of multibeam bathymetry of Hine's Hole from along with coring locations noted by grey circles, the sample location of the water column profile in b) shown by a yellow oval, and 3 Chirp subbottom seismic transect paths. Images from each transect are shown below the map panel, with raw output to the left and interpreted subbottom features noted in pink in the identical images to the right. Core names and depths are added to each image where the transect line intersects core sampling location. Panel b) in the top right provides an 87 m water column profile (temperature, salinity, pH, and dissolved oxygen) for Hine's Hole measured on 23 April 2016 sampled at 23.8652°N and 79.8048°W. (For interpretation of the references to colour in this figure legend, the reader is referred to the web version of this article.)

both the wet (April–September) and dry (October–March) seasons, with a slight secondary peak of northeasterly winds during the dry season. Using the Florida Keys Hybrid Coordinate Ocean Model (Kourafalou and Kang, 2012), Purkis et al. (2014) and Purkis et al. (2017) demonstrate that bank-top current velocity has minimal interannual variability. Purkis et al. (2017) found that annually averaged surface current velocity on Cay Sal Bank is ~0.1 m/s, approximately one order of magnitude slower than the Florida Current, thus signaling that surface flow over Cay Sal Bank is at least partially decoupled from the nearby Gulf Stream. Based on MODIS-Aqua sea-surface temperature (SST) observations from 2002 to 2011 CE, Cay Sal Bank has a mean annual SST of ~27.5 °C ± 2 °C, with highest monthly temperatures during most of the wet and peak hurricane season from June through October (~29.7 °C ± 0.5 °C), and lowest temperatures from November through May (~26 °C ± 0.9 °C) (Purkis et al., 2014).

3. Methods

3.1. Sediment collection and analysis

Visual, geophysical, hydrographic, and coring surveys were conducted aboard the *M/V Alucia* and *HOV Nadir* submersible in April 2016. A Teldyne RESON 7160 PDS2000 multibeam sonar system was used to map the bathymetry of the blue hole and surrounding rim along with the shape of the surrounding walls (Fig. 2c). Blue hole stratigraphy was mapped using an EdgeTech 3100 Chirp sub-bottom sonar system towed while sweeping at a 4–24 kHz bandwidth (Fig. 3, Supplementary Fig. S1). A YSI EXO1 portable sonde was deployed at a rate of 1 cm/s, with 2 measurements of temperature (± 0.01 °C), salinity (±0.1 Practical Salinity Units-PSU), dissolved oxygen (± 0.01 mg/L), and pH (± 0.01 pH units) collected each second (Fig. 3b).

Sediment cores (7.5 cm diameter) were collected using a Rossfelder-P3 submersible vibracorer (Figs. 3, 4a, 5), and coring location, water depth, drive length, and recovery lengths are reported in Supplementary Table S1. These drives collectively sampled up to 18 m of the stratigraphy within Hine's Hole. The sediment water interface was well preserved in Core-8 and Core-9, but the upper 110 cm of the longest recovered drive Core-7 was disturbed during the recovery process (1800 cm drive, 1627 cm recovery due to compaction and gas release). Prior to core sectioning, 3 mm diameter holes were drilled into the core pipe at ~1.45 m long increments down each core to facilitate release of interstitial hydrogen-sulfide gas for 24 h. Following gas release, each contiguous core was cut into ~1.45 m sections at each drill point. A 1728 cm long composite record, which we hereafter refer to as the Hine's

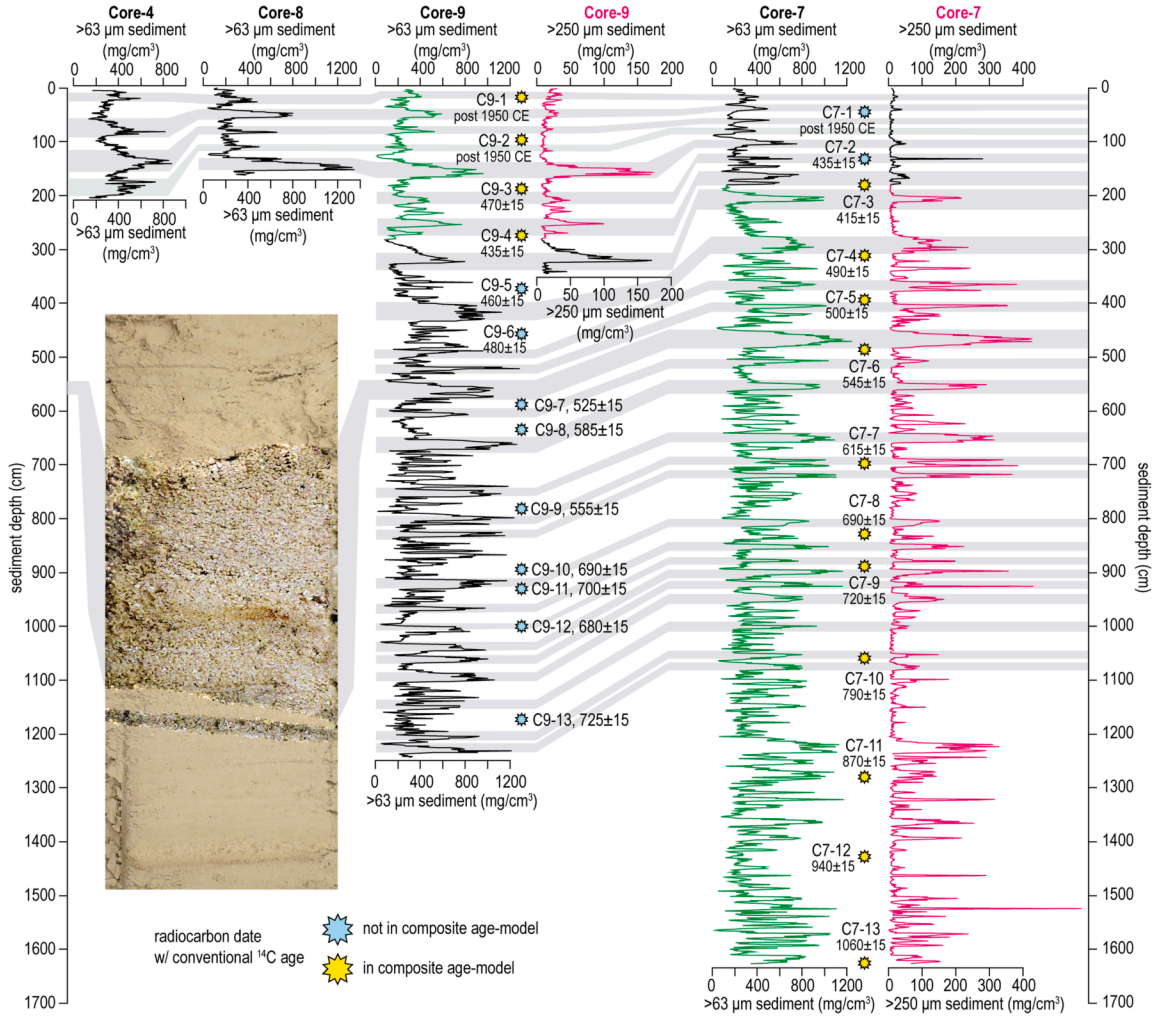

Fig. 4. Downcore sediment textural data (>63 µm mg/cm^3) for four cores from Hine's Hole, along with medium sand textural variability (>250 µm mg/cm^3) for all of Core-7 and ~ 300 cm of Core-9. The pink and green lines are the portion of Cores-7 and 9 that respectively comprise the composite Hine's Hole record at the >250 µm and > 63 size fractions. Coarse sediment layers like the one in the photograph are generally considered to be hurricane event deposits. As indicated by the grey bars, correlation of peaks is well maintained across the cores in both the >250 µm and > 63 µm size fractions. See Supplementary Fig. S3 for a detailed demonstration of the correlation of specific beds from 625 to 765 cm in Core-9 and 560 to 670 cm in Core-7. Yellow stars indicate the locations of radiocarbon dated articulated bivalves and gorgonian corals fragments that were used to develop the sedimentary age model for the Hine's Hole Composite reconstruction, whereas blue stars represent unused radiocarbon dates. (For interpretation of the references to colour in this figure legend, the reader is referred to the web version of this article.)

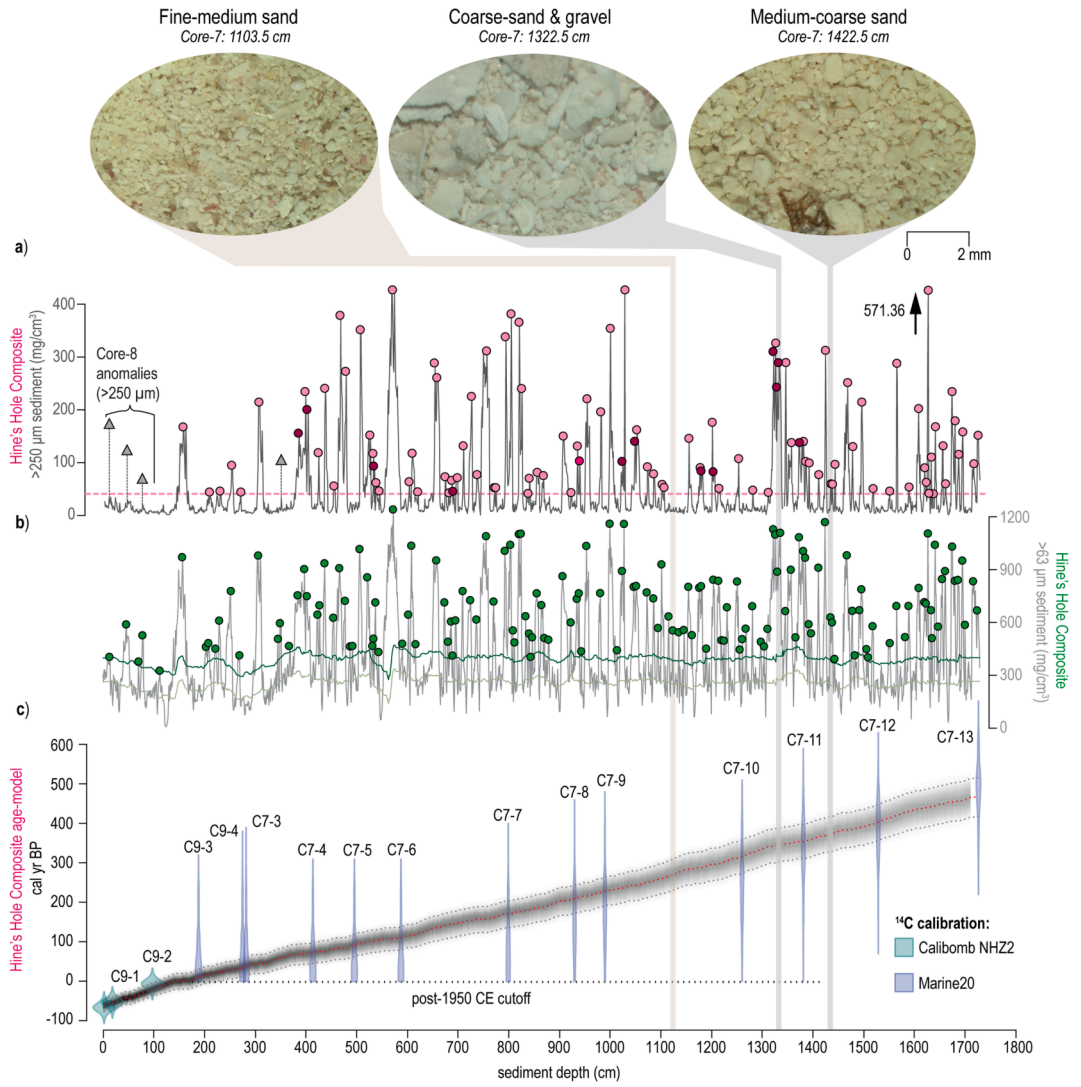

Fig. 5. Downcore sediment textural data for the a) > 250 µm (dark grey) and b) light grey >63 µm size fractions (mg/cm^3) of the Hine's Hole Composite. In a), Pink circles indicate statistically anomalous coarse event beds that exceed the 40.9 mg/cm^3 upper event bed threshold for >250 µm data. In b), green circles indicate statistically anomalous coarse event beds that exceed the 40-pt moving average (dark green line) + 150 mg/cm^3 upper event bed threshold for >63 µm data (light green line). Images above a) shows variability in particle size and composition in >63 µm sediment fractions found in Core-7. c) Sedimentary age model for the Hine's Hole Composite was constructed using 16 points of age control including 14 radiocarbon dated articulated bivalve shells leaves and 1 branch of a gorgonian soft coral from Core-7 (n = 11 dates) and Core-9 (n = 4 dates) along with a modern core-top date of 2016 CE. See Supplementary Table S2 for details on dated material. (For interpretation of the references to colour in this figure legend, the reader is referred to the web version of this article.)

Hole Composite, was made by combining the upper 280 cm of Core-9 to the point of stratigraphic equivalence in Core-7 at 180 cm, thus including the 1447 cm of Core-7 below this point (Figs. 5 and 6). These methods have been used to assemble portions of separate coring drives into single continuous sediment records for other Bahamian blue holes (Wallace et al., 2021b; Wallace et al., 2021c; Winkler et al., 2020).

In the laboratory, sediment core sections were split lengthwise to undergo high resolution photography, radiographic imaging, and textural analysis. Textural analysis and visual sedimentary characteristics facilitated downcore stratigraphic correlation between the individual drives (Fig. 5, greater detail in Supplementary Fig. S3). Sediment textural analysis was completed for each drive using a procedure similar to the sieve-first loss on ignition method described by van Hengstum et al. (2016). This technique avoids potential bias introduced by aggregating and cementing together individual fine-sediment grains through desiccation or combustion. First, a standard sediment volume of 2.5 cm^3 was sampled at contiguous 1 cm intervals downcore, then gently wet sieved over a >63 µm mesh to determine the volumetric mass of the fine-sand sized and greater particles in each subsample. The sieved residues were transferred into pre-weighed aluminum tins, then desiccated for 24 h at 85 °C. Fully dried residues were weighed to determine the mass of >63 µm sediment per unit volume (mg/cm^3) of each 1 cm subsample (Fig. 5). While this procedure does not combust bulk organic matter content, there is little bias from coarse organic matter particles on the coarse carbonate sediment deposition downcore because the stratigraphy contained negligible coarse-grained organic matter fragments. Coarse-fraction sediment residues were stored in plastic vials for use in further analysis. Subsampled residues of all Core-7 sections (1627 cm) and the first three sections of Core-9 (346 cm), which encompass all stratigraphy included in the 1728 cm long Hine's Hole Composite, were re-sieved over a >250 µm mesh following the same methods described above to constrain the ≥ medium sand size particle mass per cm^3.

3.2. Age-control

Stratigraphic age-control was developed for the Hine's Hole record using 13 radiocarbon dates from Core-7 and 13 radiocarbon dates from Core-9 (Figs. 4, 5; Supplementary Table S2). All dates were derived from

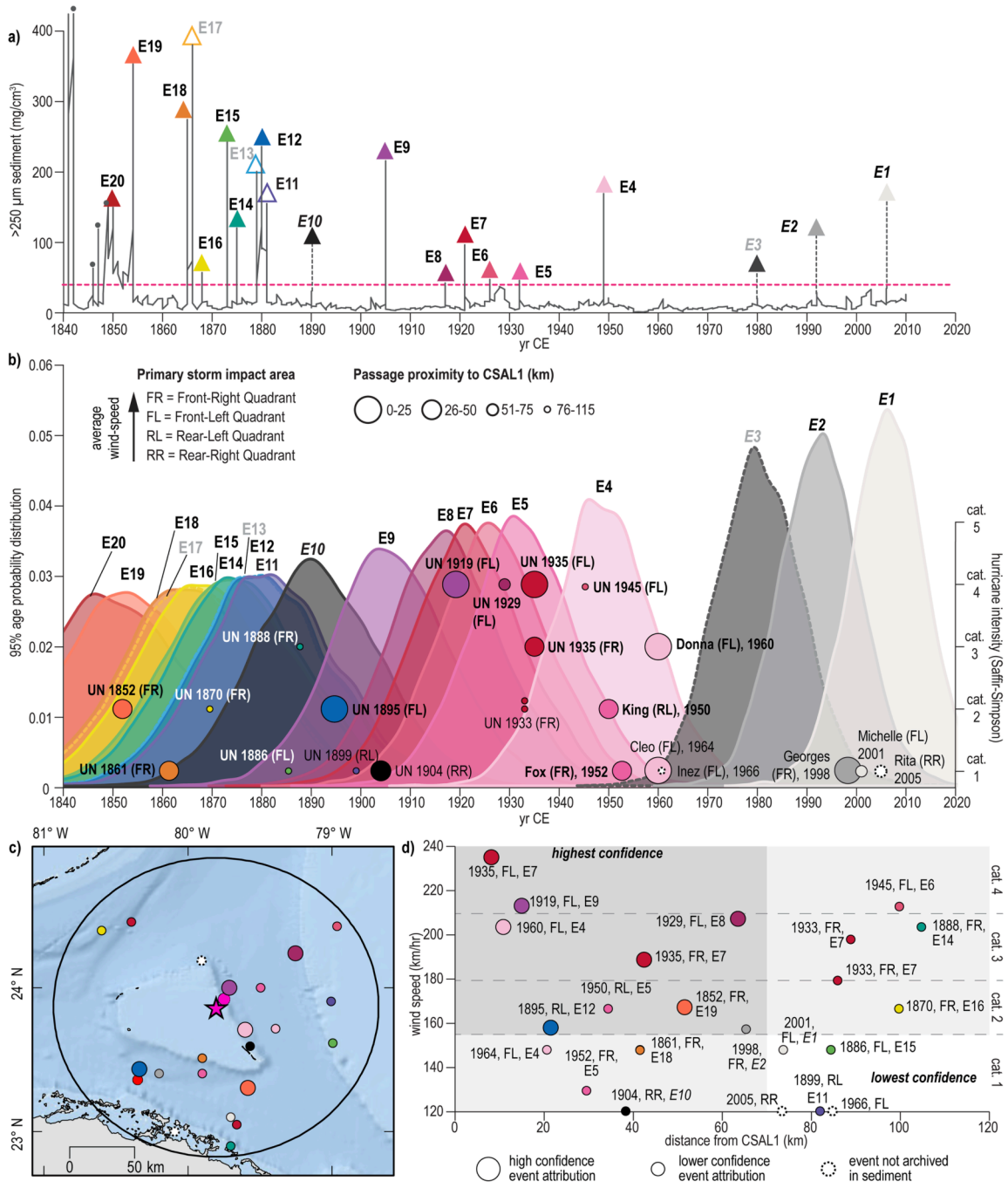

Fig. 6. a) Coarse sediment data (mg/cm^3 > 250 µm, in dark grey and > 63 µm in light grey) with >40.9 mg/cm^3 > 250 µm coarse anomaly event beds E-1, E2, E3, and E10 (from Cores-8 and 9) and E4-E19 indicated respectively by greyscale and colored triangles that correspond to the colors of 95% age probability distribution (95% PDF) plots in panel b). Only the >250 µm data was used to define hurricane event beds, but the most prominent peaks are also observed in the >63 µm data. Circles on panel b) correspond to the timing of hurricanes observed within 115 km of Hine's Hole from 1850 to 2015 CE ($n = 23$). Circle diameter is proportional to passage proximity (larger circle = closer passage), and vertical position of the circles corresponds to the intensity of the storm on the Saffir-Simpson hurricane scale (right y-axis). Circle colour corresponds to the colour of the 95% PDF plot of the event bed that the observed hurricane event is most likely associated with (modern hurricanes with no associated event bed in the Hine's Hole Composite are solid black. Panel c) includes a map of the point of closest passage to Hine's Hole of all hurricanes from 1850 to 2015 CE depicted in panel b), with colour associated with the coarse anomaly that is attributed to the hurricane event and the size and shape corresponding to the confidence in that attribution (see legend). Applying the same symbology, d) is a scatterplot of the wind speed of each of these hurricanes plotted against to the distance of closest passage to Hine's Hole. This diagram shows that over the last ~170 years, Hine's Hole reliably archives most ≥Category 1 hurricanes within 75 km and most ≥Category 2 hurricanes within 115 km depending on the angle of approach.

the outer growth ring of articulated bivalve shells belonging to the *Tellinidae* family, save for one date derived from a gorgonian coral branch from the base of Core-7 (1627 cm). All dated material was extracted from the core then cleaned using ultrasonic vibrations in a deionized water bath. Samples were then rinsed over a > 250 µm mesh to remove any remaining sediment, then dried overnight at 85 °C. Bivalve shells were de-articulated using ethanol sterilized tweezers, and ~ 2 mm wide sections of the outermost/youngest growth rings were cleaved away to be dated. All radiocarbon dating was completed by the National Ocean Sciences Accelerator Mass Spectrometry facility at

Woods Hole Oceanographic Institution, where samples were hydrolyzed prior to measurement of radiocarbon abundance and $\delta^{13}C$ ratios using accelerated mass spectrometry.

Based on the high $\delta^{13}C$ measured for each mollusc and coral sample, conventional radiocarbon dates were calibrated into years before present (cal yr BP) using the Marine20 calibration curve (Heaton et al., 2020). This calibration provides a global mean correction of 550 years to address residence time of radiocarbon within marine reservoirs prior to bioassimiliation by marine organisms that build on the atmospheric correction provided by IntCal20 (Reimer et al., 2020). As discussed and illustrated in detail in Supplemental 4, no additional reservoir (ΔR) correction was applied to these samples as the marine reservoir variability on Cay Sal Bank has not been constrained given that no regional correction value has been established in the literature. Three samples from the upper 100 cm of Cores-7 and 9 with fraction modern carbon value ($F^{14}C$) in excess of 1 were calibrated using the Northern Hemisphere Zone 2 dataset (NHZ2) from the free online resource CALIbomb (Reimer et al., 2004).

Fifteen of these radiocarbon dates, 4 from Core-9 and 11 from Core-7, and a modern age of 2016 CE at the core-top were used as age-control points in a sedimentary age model (Fig. 5) that was developed using Bayesian statistical approaches in the R library Bacon v2.3 (Blaauw and Christen, 2011). The age model only includes age-control points from the core sections that were included in the Hine's Hole Composite (i.e., upper 280 cm of Core-9 and lower 1447 cm of Core-7), and ages were estimate downcore for every 1 cm stratigraphic level for the Hine's Hole Composite. Based on the results (see below), we assume that thick (>2 cm), coarse-grained stratigraphic units with >40 mg/cm^3 of 250 μm were deposited instantaneously, most likely by heightened hydrodynamic conditions related to severe weather events such as hurricanes. As such, these coarse layers were designated as geologically instantaneous events using the SLUMP command in Bacon v2.3, which groups the entire specified layer into a single year in the age model output (101 SLUMP entries were defined, accounting for a total of 665 cm with an average thickness of 6.6 cm ± 4.3). Using the same parameters and control points, we also developed an alternate age model to test the temporal effects of using a reservoir correction of $\Delta R = -92 \pm 111$, which was found to be the weighted mean of the 40 most proximal ΔR values from the literature, which ranged from 150 to 360 km away from Hine's Hole (Supplemental 4, Supplementary Fig. S4; (Broecker and Olson, 1961; Diaz et al., 2017; DiNapoli et al., 2021; Druffel and Linick, 1978; Druffel, 1997; Hadden and Schwadron, 2019; Lighty et al., 1982). As discussed in Supplemental 4 this age model was not used because it introduced significant uncertainty regarding the reservoir correction. However, this alternate age model did indicate that even an aggressive reservoir correction of $\Delta R = -92 \pm 111$ would have minimal influence on the median/mean predicted ages (<50 years).

3.3. Event attribution and frequency calculation

Coarse sediment anomalies that are likely indictive of high-energy event transport/deposition were identified as significant "event beds" if the fraction of coarse sediment >250 μm mg/cm^3 exceeded a threshold of 40.9 mg/cm^3 derived following the Tukey rule of outlier detection for exponentially distributed data (Tukey, 1977). The Tukey rule states that outliers are values that fall above the third quartile (*Q3*) or below the first quartile (*Q1*) by at least 1.5 times the interquartile range (*IQR*) of the dataset (Eq. 1). This outlier threshold was calculated by determining the mean value of all >250 μm mg/cm^3 points that fell below 50 mg/cm^3, which is the *lower ~ 75th percentile* of the cumulatively distributed >250 μm fraction ($n = 1257$), to estimate the average volumetric mass of non-event sedimentation (16.46 mg/cm^3), resulting in a rate parameter of $\lambda = 0.061$.

$$Tukey\ rule\ for\ outliers = Q3 + 1.5IQR \quad (1)$$

$$Q1 = -ln0.75/\lambda;\ Q2\ \text{or}\ mean = 1/\lambda;\ Q3 = -ln0.25/\lambda;\ IQR = Q3 - Q1$$

The highest mg/cm^3 value from a single coarse event bed in excess of this threshold was counted as the event depth if the event bed was thicker than 1 cm. In the conservative event counting, event beds were considered independent from one another if they were separated by diminishing values for at least 2 cm provided at least one of these values either: i. fell near or below the 40.9 mg/cm^3 threshold, ii. was <50% of the value of the highest peaks on both sides of the bed, or iii. Could be differentiated by visual sedimentary characteristics (i.e., coarse vs. fine grains and colour; Figs. 5–7). In the more liberal event counts, beds were considered distinct if they were separated by more than 2 cm of sediment wherein 250 μm mg/cm^3 values diminished by at least 30% of the highest value on either side (Figs. 5–7).

Separate procedures were followed to calculate the >63 μm mg/cm^3 anomalies based on the methods of Donnelly et al. (2015). A 40-point moving average was calculated for >63 μm data, excluding values that exceeded 400 mg/cm^3. This moving average was subtracted from the >63 μm mg/cm^3 data to isolate coarse sediment anomalies. Similar to the liberal >250 μm event counts, only the highest value point from each coarse bed was counted, and beds were s considered distinct if they were separated by more than 2 cm of sediment wherein mg/cm^3 values diminished by ~30% of the highest value on either side (Fig. 5b, Supplementary Fig. S7).

Following the methods of Winkler et al. (2020), hurricanes from 1850 to 2016 CE documented in the IBtRACS v4 dataset (Knapp et al., 2018; Knapp et al., 2010) were attributed to event beds in the upper portion of the Hine's Hole Composite where event beds median 2σ age was between 1850 and 2016 CE (Fig. 6, Supplementary Tables S3, S4). Hurricanes within the 2σ age-range of the event bed were considered as potential depositional drivers if they passed within 115 km of Hine's Hole, which was selected based on the geographic exposure of Hine's Hole as well as the recording sensitivity of other Bahamian blue hole records (Wallace et al., 2021b; Wallace et al., 2021c; Winkler et al., 2020). We also considered tropical storms if no hurricanes could be readily attributed to event beds. We acknowledge that locally severe winter storms may also produce coarse-sediment deposits, but documentation of intensity, track, and timing for these storms is less comprehensive in the instrumental record, so we focus our attribution analysis on hurricane strength storms. Starting with the most recent event bed, *E1*, we identified the event(s) that had the highest probability of generating each event bed based on factors such as the median age of the deposit, the intensity and proximity of the storm to Hine's Hole, the relative age/depth separation between sequential event beds vs the temporal window between historic storms, and which quadrant of the storm had the dominant impact during passage (Fig. 6, Supplementary Tables S3, S4). This calibration process was used to verify the accuracy of the event bed detection thresholds as well as providing context for what types of storms are most likely to be recorded by Hine's Hole throughout the paleo-record.

After calibrating the site sensitivity and verify thresholds, event beds were counted in both the >250 μm and >63 μm datasets using 50 and 100-year sliding windows following the methods of Lane et al. (2011), wherein the number of coarse sediment anomalies within 25 or 50 year windows (before and after) of each 1 cm interval is counted (Fig. 7, Supplementary Fig. S7). Both temporal windows were normalized to hurricanes/century to assess centennial-scale hurricane variability, but the 50-year sliding window counts likely emphasize shorter periods of extremely high or low hurricane activity that are variable at a multi-decadal scale.

Active intervals with significantly elevated hurricane frequency are defined using the site-specific threshold calculations detailed by (Lane et al., 2011; Wallace et al., 2019), wherein we assume hurricane impact frequency follows a Poisson process, meaning that the individual storms are discrete events for which timing and location is not impacted by the

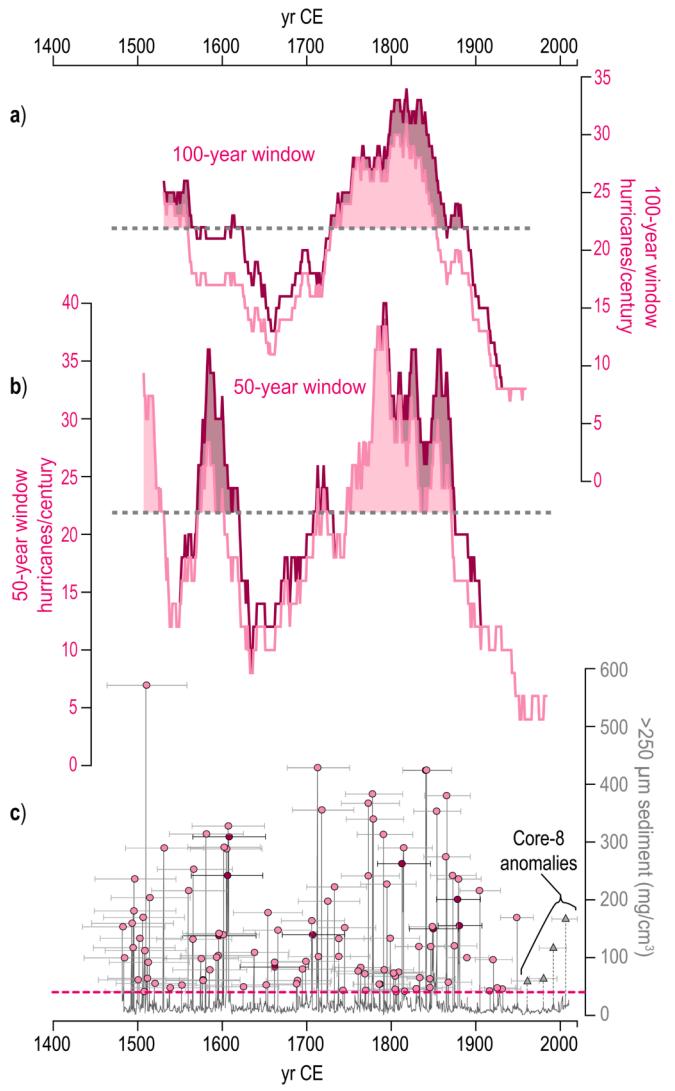

Fig. 7. a) The pink/maroon lines represent 100-year moving window counts for >250 µm event beds per century in the Hine's Hole Composite at the conservative (pink) and liberal (maroon) counting methods. The pink conservative lines are plotted in front of the maroon liberal lines, so the conservative and liberal counts are in full agreement when only the pink line is seen. The site-specific upper threshold for a statistically active interval, >21.9 hurricanes/century (≥Category1 within 115 km), is marked by a dashed grey line in both the 100- and 50-year window counts. Temporal windows where hurricanes/century exceed this limit are shaded in pink (conservative) or maroon (liberal). b) Same as a), but lines represent the 50-year window counts which were doubled to normalize to hurricanes/century. c) > 250 µm coarse sediment anomalies (grey line) from Hine's Hole Composite from 1460 to 2016 CE. The pink dashed line is the 40.9 mg/cm^3 anomaly threshold, and event beds that exceed this threshold are marked with pink circles (maroon for liberal only bed). 2σ (95%) age-uncertainty windows for each coarse anomaly are shown by the horizontal black error bars.

incidence of other storms. Based on the site sensitivity calibration, most of the 23 total ≥ Category 1 hurricanes within 115 km since 1850 CE left a significant event deposit in the Hine's Hole Composite at a rate of 13.9 hurricanes/century (see Discussion section *5.3 Changing event frequency*). Based on this rate, we calculate an upper 95% significance threshold of 21.9 hurricanes/century following the procedures of Ulm (1990), meaning that any activity levels above this threshold are unlikely to be driven by random variability in storm tracks alone (Fig. 7). We acknowledge that this estimate of significance could be an underestimate as it does not include the number of severe winter storms or proximal tropical storms since 1850 CE; however, this estimate does count multiple ≥ Category 1 hurricanes within the same year (i.e., 2 events in both 1933 and 1935 CE) despite the fact that these deposits are likely indistinguishable from one another based on the sedimentation rate and sampling resolution. We therefore stress that this is simply a means of estimating significant temporal variations in the record, and that any values at the fringe of this threshold should be interpreted cautiously.

4. Results

4.1. Geophysical and hydrographic survey

The rim of Hine's Hole sits at an average depth of ~10 m (Fig. 2c) and is partially surrounded by a 0–2 m thick veneer of sandy sediment. Hine's Hole appears to have vertical karst walls around the North, East, and West flanks, and a ~ 45° downward slope along the south flank that extends ~100 m before flattening out to a ~ 5° deepening northward slope (Fig. 2c). No cave passages were observed during direct human observations aboard the Human Operated Vehicle (HOV) Nadir submersible. The water column is slightly stratified in Hine's Hole, with a moderate pycnocline from 50 to 60 m (salinity change: 40.4 to 41 psu), below which dissolved oxygen decreases to a minimum of 2 mg/L (Fig. 3b). This suggests that the basal water mass in the blue hole is at least partially sheltered wave-induced mixing and surface currents. However, the levels of dissolved oxygen are still sufficient to support a benthic ecosystem, as indicate by invertebrate burrows in the fine-grained benthic sediment (Supplementary Fig. S2) Overall, the base of Hine's Hole gently slopes from ~80 m along the southern base to ~95 m along the northern margin (Figs. 2c, 3). Seismic subbottom surveys conducted for this study in 2016 for this confirm the observations of Hine and Steinmetz (1984) for thick sediment accumulations across the bottom of the blue hole, with internal acoustic reflectors visible in the top 5 m of the accumulation that likely indicate variance in sediment style or composition that signal a change in impedance (Fig. 3, Supplementary Fig. S1). A sloping, relatively continuous hard reflector can be observed from 20 to 60 m below the sediment surface at the base of the hole. Strata between the upper and lower reflectors is obscured, likely because of high levels of interstitial gas (e.g., hydrogen sulfide or methane) that attenuates the acoustic energy during transmission. These results suggest that the blue hole contains at least a 60 m stratigraphic sequence, with the thickest accumulation in the deeper north-central area. Hine and Steinmetz (1984) observed higher levels of sediment deposition along the eastern flank of the blue hole. However, expanded sediment accumulation in the eastern portion of Hine's Hole is not supported by the relatively flat bathymetry across the sediment surface in Hine's Hole (Fig. 2c), nor is it evident in the new subbottom reflectors from the Chirp surveys (Fig. 3a, Supplementary Fig. S1). Therefore, it is likely that sediment is well dispersed in the water column before settling out of suspension evenly across the benthos in this natural settling column.

4.2. Sedimentology and age-control

Recovered sediments reveal that Hine's Hole predominantly traps carbonate mud and fine sands that are likely deposited during relatively quiescent hydrodynamic conditions. Fine-grained carbonate mud was not found in previous bank top sedimentological surveys (Goldberg, 1983; Hine and Steinmetz, 1984; Purkis et al., 2014) or in the sediment grab samples collected from the periphery of Hine's Hole for this study. However, fine grained sediments were observed settling-out of suspension from the water column during an exploratory dive in the *HOV Nadir* submersible in 2016 (Supplementary Fig. S2c-f). The fine-grained carbonate mud intervals in Hine's Hole are not continuously laminated like the anoxic Great Blue Hole on Lighthouse Reef Atoll in Belize (Gischler et al., 2008), so they are not conducible to developing an independent,

varve-based age model (e.g., Denomee et al., 2014; Schmitt et al., 2020). These finer-grained muds and fine sands are interrupted by numerous coarse-grained sediment beds (texture: medium to coarse-sand) in the stratigraphy that are rich in skeletal material, pelloids, and weathered karst fragments. Despite the dissolved oxygen concentrations at the benthos being able to support some benthic invertebrates (Supplementary Fig. S2h), sharp contacts between the coarse and fine stratigraphic layers and occasional laminations are observed (Fig. 4, Supplementary Fig. 3). Horizontal bedding and lack of homogenization together suggest negligible post-depositional bioturbation or current driven reworking of sediments and of this primary textural signal. The denser and coarser sand layers are visually distinct, and textural analysis distinguishes the sharp contacts between sandy-mud background facies and these medium to coarse-sand deposits (Fig. 4). These coarser sediments dominate the sand deposits currently found on the bank-top (Figs. 2, 4, 5; Purkis et al., 2014). Overall, organic matter particles were visually scarce in both the fine and coarse lithofacies, but where observed, were composed of fragmented sea grass blades and small clusters of green macroalgae.

The coarse beds and other features like occasional laminations could be stratigraphically correlated between cores using high-resolution photographs and the textural data throughout the overlapping portions of each of the four cores (Fig. 4, Supplementary Fig. S3). Based on this correlation analysis, the first 280 cm of Core-9 represent a complete and often expanded (i.e. thicker lithologic units) sequence that correlates to the first 180 cm of Core-7 (Fig. 4), with the length discrepancy likely resultant of sediment that was lost or highly disturbed during the recovery process of Core-7. Similarly, coarse bed stratigraphy in the 162 cm Core-8 (the best-preserved recovery of the upper meter of sediment) reproduces that of the first 190 cm of Core-9. Core-4 also shows many stratigraphic similarities to these three cores but was collected ~100 m westward of the other cores and appears to archive thicker coarse beds likely due to higher sediment accumulation given its proximity to the rim of the blue hole. As such, portions of each of Cores-7, 9, and 8 were compiled to assemble the 1728 cm long Hine's Hole Composite (Figs. 4 and 5a, b). The first 280 cm of Core-9 was used as the upper portion of the Hine's Hole Composite, with 180–1627 cm in Core-7 (1447 cm) forming the rest of the 1728 cm long composite record. This point of merging is further supported by two radiocarbon dates from Cores-9 and 7 at depths of 273.5 cm (C9–4) and 179.5 (C7–3) cm in the Hine's Hole Composite, where the conventional radiocarbon ages are 435 yr BP ± 15 yr BP and 415 yr BP ± 15 yr BP (Fig. 5, Supplementary Table S2). Conventional radiocarbon dates in the deeper portions of Cores-9 and 7 support the accuracy of the visual stratigraphic correlations that were made between these two cores (Fig. 4, Supplementary Table S2). No age-control points were obtained for Core-8 so no continuous portions of it were used in the Hine's Hole Composite; however, >63 μm coarse peaks in Core-8 were re-sieved over a > 250 μm mesh to determine the fractional mass of the coarse sediment in these beds. Core-8 is much shorter, so the coring process was much faster, meaning that it was not exposed to prolonged vibrations from the coring motor that can homogenize less-consolidated sediment for the same duration as Cores-7 and 9.

The >250 μm dataset had an average coarse sediment fraction of 48.6 mg/cm^3 ± 68.5, and 96 coarse sediment deposits exceeded the threshold of 40.9 mg/cm3 and were identified as coarse sediment anomalies using the conservative counting methods, while 106 coarse sediment anomalies identified using the liberal counting methods (Fig. 5a). Four additional event beds were identified (E1 to E3) in Core-8 and Core-9 (E10) that exceeded the significance threshold, whereas stratigraphically correlated coarse-sediment beds in the Hine's Hole Composite were less pronounced and did not exceed the significance threshold (Figs. 4 and 5). These additional event beds bring the total to 100 and 110 for the conservative and liberal event counts, respectively. The >63 μm dataset had an average coarse sediment mass fraction of 422.2 mg/cm^3 ± 241.1, and 148 event beds were identified as coarse sediment anomalies based on the thresholds discussed in section *3.3 Event attribution and frequency calculation* (Fig. 5b). Anomalous coarse-bed thickness ranged from 1 cm to ~25 cm in both the >250 μm and >63 μm size fractions, with an average thickness of ~6.1 cm in the >250 μm dataset.

Sedimentation in Hine's Hole has been approximately linear with an average sedimentation rate of 2 cm/yr from 1480 to 2016 CE based on the Bayesian statistical age model (Fig. 5c). This sedimentation rate represents an estimate of the background, non-event driven sedimentation rate that was calculated by labelling all coarse deposits ≥2 cm in thickness as instantaneous events during age model development (background sedimentation accounts for ~1053 cm in the >250 μm dataset). If these events are not excluded, the overall sedimentation rate of the 1728 cm Hine's Hole Composite is ~3.2 cm/yr. Age model uncertainty is lowest from 0 to 524 cm (1850-2010 CE), where the average uncertainty is ±21.4 years (standard deviation ±4.1). Below this, uncertainty increased linearly with depth and time, averaging ±39.1 years (standard deviation ±5.9) .

5. Discussion

5.1. Age-model limitations and implications

MarineCal20 calibrated median-ages of control points from Core-9 (C9–3, C9–4) and Core-7 (C7–3, C7–4, C7–5, C7–6) are more recent than 1950 CE when no ΔR correction is applied, despite none of these having fraction modern ^{14}C values >1 (i.e., no post-1950 CE thermonuclear radiocarbon). For dates C7–7 through C7–13 from Core-7, Marine20 calibrated median ages fall prior to 1950 CE and the average background sediment accumulation rate of 2 cm/yr (3.2 cm/yr including coarse beds) falls within higher confidence age- range estimates for these control points (Fig. 5c). The fact that the median age of the first six non-modern ^{14}C rich samples is calibrated beyond 1950 CE suggest that some additional negative ΔR correction is needed to correct for a local marine reservoir that is likely younger than the 550 year global marine reservoir used in the Marine20 calibration curve (Heaton et al., 2020). However, no ΔR correction values currently exist for Cay Sal Bank, and high-levels of interspecies and regional variability in ΔR corrections across the Caribbean means that applying any sort of regionally-averaged ΔR correction introduces additional uncertainty (Supplemental 4; DiNapoli et al., 2021; Toth et al., 2017). Further, based on the work of Kondo (1987), the pallial sinus index of the Tellinidae bivalve specimens we dated (~0.3 based on 10 measured specimens) suggests that these organisms burrow their approximate body length into the sediment, meaning that dated organisms are likely to be stratigraphically young relative to surrounding sediment at the burrow depth. As such, we assume that adding any additional ΔR correction presents greater uncertainty than just correcting to the global marine reservoir value alone.

Regardless of uncertainties, the sedimentation rate in Hine's Hole is exceptionally high relative to other subtidal Bahamian blue holes, which tend to fall between 0.6 and 1.3 cm/yr (Wallace et al., 2019; Wallace et al., 2021b; Wallace et al., 2021c; Winkler et al., 2020). Given that the average current depth of Cay Sal Bank around Hine's Hole is ~10 mbsl, Hine's Hole likely became an inundated marine depositional environment that is analogous to modern depositional conditions around ~8000 yrs. BP (range 7000–10,000 yrs. BP) based on the Bahamas sea-level curve compiled by Khan et al. (2017). If we assume that: i. the average sedimentation rate of ~3.2 cm/yr calculated for the upper 18 m of stratigraphy (carbonate mud and multiple storm-driven carbonate sand layers) is constant through time, and ii. sedimentary processes have remained similar throughout the inundated marine phase which likely persisted since the bank top flooded ~11,000 to 6000 years ago (Purkis et al., 2014), then the ~60 m of accumulation that is observable in the Chirp surveys (Fig. 3, Supplementary Fig. S1) could represent just ~1900 years of sediment accumulation in Hine's Hole.

5.2. Calibrating the record to historical hurricanes

Based on the median date derived from the age model, the upper ~520 cm of the Hine's Hole Composite represents to the period from 1850 to ~2016 CE. During this time, there are 20 coarse sediment anomalies in the >250 μm size fraction that exceed the 40.9 mg/cm^3 significance threshold including the 4 additional anomalies that were only detected in correlated beds from Cores-8 or 9 (E1-E3 and E10, Figs. 4–6). Based on the punctuated nature of these coarse-sediment beds, it is likely that these anomalies were deposited by heightened currents or waves that are generated during extreme events like storms and tsunamis. As discussed by Winkler et al. (2020), tectonic sources (i.e., tsunamis) are unlikely to play a major role in causing extreme waves in the region around The Bahamas. The Azores–Gibraltar plate boundary is the most likely tectonic origin of major tsunamis that could impact The northern Bahamas, such as with the 1755 CE Lisbon Earthquake, for which numerical models predict far-field wave heights of less than 1 m in the northern Caribbean (NCEI/WDS Global Historical Tsunami Database; (Arcos et al., 2018; Barkan et al., 2009). Further, it is likely that the Little Bahama Bank buffered these waves resulting in a diminished impact with modelled wave amplitude of <0.2 m across Cay Sal Bank (Arcos et al., 2018). Even if a tsunami from a strong event like the 1755 CE Lisbon Earthquake could deposit a coarse sediment bed in Hine's Hole, the tsunami recurrence interval in The Bahamas is on the order of ~500 years (Parsons and Geist, 2008) compared to the decadal recurrence of intense hurricanes throughout the region. Given that we are interested most in long-term variability illuminated by high-resolution sediment records, as opposed to interpreting a single event bed as climatically deterministic, tsunami induce coarse deposits likely have negligible impacts on the derived temporal trends and interpretations in this study.

A relatively comprehensive instrumental record of North Atlantic tropical cyclone activity (e.g., timing, track, wind speed, pressure) from 1850 to 2020 CE is compiled by within the IBtRACS hurricane database, which is most reliable following widespread implementation of satellite observation in the 1960 CE and is considerably less reliable prior to the use of air-craft storm monitoring in the 1940s (McAdie et al., 2009; Vecchi and Knutson, 2011). As described in the methods, we initially assumed that hurricanes of at ≥Category 1 strength passing within 75 km of Hine's Hole may be capable of generating a coarse deposit in the sedimentary record. However, only 15 hurricanes since 1850 CE meet these criteria, and four of these events fall within separate two-year periods and are likely indistinguishable in the sedimentary record (Fig. 6, Supplementary Tables S3, S4). As such, the proximity threshold was expanded to ≥Category 1 strength within 115 km since 1850 CE. This proximity threshold includes 23 possible hurricanes (Supplementary Fig. S5) of which 5 hurricanes separated by less than 2 years that may not be distinguishable in the sedimentary record based on how some hurricanes may impact coarse sediment supply around Hine's Hole (18 total). Starting with the most recent deposits and working backward through time, these 18–23 historical hurricanes from 1850 to 2016 CE were assessed as emplacement mechanisms for each of the 20 > 250 μm coarse-sediment anomalies based on age-range, proximity, wind-speed, and angle of approach (Fig. 6, Supplementary Tables S3 and S4). To understand this process, Supplementary Tables S3 (1900–2016 CE) and S4 (1850–1899 CE) list characteristics of all ≥Category 1 hurricanes passing within 115 km of Hine's Hole that fall within 2σ age range of each >250 μm coarse-sediment anomaly of the last ~170 years (Fig. 6a, b). In Fig. 6b, the 95% (2σ) age probability distribution functions are plotted for each coarse anomaly, and the strength and timing of historical storms overlay this to demonstrate which events could be responsible for each deposit based on the sedimentary age model. Finally, Fig. 6c shows the most proximal passage for each storm to Hine's Hole, and Fig. 6d plots each historical event by passage distance vs wind speed to show what types of storm characteristics are most associated with attributed hurricanes.

Deposit E1 has a median-age of 2006 CE and a 2σ range = 1991–2021 CE. The next deposit, *E2*, has a median age of 1992 CE and a 2σ range of 1976–2008 CE. The only hurricanes within 115 km of Hine's Hole during the age-uncertainty range of these two deposits are Rita in 2005 (Category 1, 71 km), Michelle in 2001 (Category 1, 73 km), and Georges in 1998 CE (Category 1–2, 65 km). Rita only developed into a very weak Category 1 hurricane after it passed Hine's Hole (max wind speed ~120 km/h), which was exposed to even weaker winds in the rear-right quadrant of the storm. As such, the most likely sources of E1 and E2 are, respectively, Hurricanes Michelle (2001 CE) and Georges (1998 CE) (Fig. 6, Supplementary Table S3). Moving downcore, E3 has a median date of 1980 CE with a 2σ age range of 1964–1997 CE, during which time three hurricanes, Cleo (1964 CE, Category 1) and Donna (1960 Category 3), and tropical storm (Greta, 1970 CE) passed within 30 km of Hine's Hole with the site exposed to the front left quadrant of the storm. Additionally, Hurricane Inez passed within 85 km of Hine's Hole in 1966 as a Category 1 storm. Based on the ~15-year separation between the median ages of E2 and E3 and the relatively small fractional mass of >250 μm sediment of E3 (~65 mg/cm^3), it is likely that weaker TS Greta (1970 CE) or the more distal Hurricane Inez (1966 CE) was the source of E3.

Proximal hurricane passage was generally more frequent prior to 1970 CE, so we will only discuss the most likely event deposit sources here; however, the comprehensive list of hurricanes since 1850 CE can be viewed in Supplementary Tables S3 and S4. Coarse anomaly E4 (median age 1949 CE; 2σ range 1930–1969 CE) is the most prominent-coarse deposit in the upper 300 cm of sediment. Deposit E4 has a relatively high proportion of >250 μm sediment, with a maximum value of 169.4 mg/cm^3 in the 23 cm thick deposit. In contrast, E3 has a maximum 250 μm fractional mass 64 mg/cm^3 and is only ~3 cm thick. As such, E4 is most likely attributed to a locally intense event, like Category 3 Hurricane Donna, which passed within 11 km of Hine's Hole in 1960 CE. That said, event bed thickness or >250 μm coarse sediment mass is not always directly indicative of overall storm intensity as local storm intensity is also influenced by variables like proximity, angle of approach, translation speed, storm size; however, Hurricane Donna and TS Greta followed a similar east to west path to the north of Hine's Hole, but Donna was 20 km closer and had at least 120 km/h faster winds. As such, Hurricane Donna was likely responsible for a more notable E4 coarse sediment deposit. This high confidence attribution of E4 to Hurricane Donna suggests that there is at least a ≥ 10-year offset in median age estimates at this point in the record, which manifests in other attributions shown in Fig. 6. This is likely resultant of the greater age-uncertainty associated with the Marine20 calibration curve as well as the potential need for a modest ΔR correction.

Median ages of coarse anomalies E5-E8 are clustered between 1935 and 1915 CE, and likely represent several decades of relatively high activity. The cumulative 2σ age uncertainty of these deposits is from 1895 to 1954 CE, during which time 11 ≥ Category 1 hurricanes passed within 115 km of Hine's Hole, including four major hurricanes in 1935 CE and 1933 CE (two each year). Based on this, E5 (median age 1932 CE; 2σ range 1911–1954 CE) is most likely attributed to one or both Category 2 Hurricane King which passed within 34 km in 1950 CE or Category 1 Hurricane Fox whose front right quadrant passed within 30 km of Hine's Hole in 1952 CE. Chronologically, E6 was most likely deposited by a Category 4 hurricane whose front left quadrant passed within 100 km of Hine's Hole in 1945 CE. Deposit E7 was likely deposited by one or more of the two Category 4 and 3 hurricanes in passing within 8 and 43 km of Hine's Hole in 1935 CE, as well as the Category 3 and 2 hurricanes that passed within ~85–90 km in 1933 CE. Though the magnitude of the >250 μm sediment mass (mg/cm^3) is relatively low despite the high intensity and close proximity of these storms, it is possible that the first of these major hurricanes washed sediment accumulations off the bank-top leaving minimal time for new sand banks to accumulate around Hine's Hole between each storm. Depleted bank-top coarse sediment supply following the two hurricanes in 1933 CE could explain why two

distinct coarse sediment anomalies are not observed for both the 1933 CE and 1935 CE hurricane clusters, even though ~4 cm of carbonate mud should have accumulated between the 1933 and 1935 CE events based on the 2 cm/yr background sediment accumulation rate. Deposit E8 has a median age of 1917 CE (2σ range from 1895 to 1940 CE), just four years before E7, meaning it was most likely deposited by the Category 3 hurricane on 27 September 1929, which is the last major hurricane event in this 20-year cluster.

Following E8, only E9 had median age more recent than 1900 CE (Fig. 6, Supplementary Table S3). The only hurricanes within 115 km of Hine's Hole during this time were a Category 4 hurricane passing within 15 km in 1919 CE and a weak Category 1 hurricane within ~40 km in 1904 CE. Deposit E9 has a median age of 1905 CE with 2σ range of 1882–1930 CE, meaning it occurred ~10 years prior to E8 which was attributed to a hurricane in 1929 CE. Based on the timing, the relatively high fractional mass of >250 μm sediment (216 mg/cm^3), and the lack of event beds within ±10 years of E9's median age, E9 was likely deposited by the proximal Category 4 hurricane in 1919. This means that the weak Category 1 hurricane in 1904 CE is likely deposited the relatively less coarse E10.

Ten additional coarse anomalies have median ages ranging from 1850 to 1881 CE (E11-E20), which had a cumulative 2σ age-range of 1822–1908 CE (Fig. 6, Supplementary Table S4). During this time, the IBtRACS database documents just seven ≥Category 1 hurricanes within 115 km of Hine's Hole. We attribute these 7 hurricanes to the >250 μm coarse sediment anomalies on a mostly chronological basis, with the only confident attributions being: i. E12 (median age 1880 CE) likely deposited by a Category 2 hurricane within 20 km in 1895 CE, ii. E18 (median age 1865 CE) being deposited by front right quadrant Category 1 winds within 42 km in 1861 CE, and iii. E19 (median age 1854 CE) being deposited by front right quadrant Category 2 winds within 42 km in 1852 CE. Deposits E13, E17, and E20 did not have clear attributions to hurricanes within 115 km of Hine's Hole. Given the technology prior to 1900 CE along with the remote nature of Cay Sal Bank, it is possible that these deposits were produced by unrecorded tropical cyclones or very intense winter storms or even a more distal hurricane like Category 1 hurricane in 1891 CE, which passed within 175 km of Hine's Hole. It is also possible that these deposits represent overcounts as both E13 and E17 were identified using the liberal counting method (Figs. 5a, 6a; see Methods).

Collectively, this event attribution exercise reveals that 17 of the 20 > 250 μm coarse sediment anomalies with median ages from 1850 to 2016 CE may be attributed to ≥Category 1 hurricanes that pass within 115 km of Hine's Hole throughout the instrumental record (Fig. 6). As discussed above regarding event beds E3 and E4, stratigraphic thickness of storm deposits may be related to the local intensity of waves produced by the storm event. Studies have demonstrated that the thickness of coarse-sediment event deposits in lakes is indicative of the volume of mobilized sediment during a flood, and is therefore a reliable proxy for estimating flood intensity (Sabatier et al., 2017; Wilhelm et al., 2015). Attempts have been made to utilize the thickness of event beds in blue holes to estimate the intensity of past hurricanes (Denomee et al., 2014; Schmitt et al., 2020). We assess the suitability of this proxy for estimating the local intensity of hurricanes near Hine's Hole over the last ~170 years that we attribute to deposits E1-E20 by dividing the maximum wind speed of the hurricane by the closest distance of passage to Hine's Hole to estimate relative intensity (Supplementary Tables S3 and S4). We find a weak positive correlation between relative intensity and event bed thickness in the 17 event beds that we attribute to hurricanes (r = 0.6; Supplementary Fig. S6). This relationship is best observed in deposits E4, E7, and E9, which are all attributed to major hurricanes (≥Category 3) hurricanes within 15 km of Hine's Hole that represent the 3 hurricanes with the highest estimated local relative intensity over the last ~170 years. It is therefore likely that event bed thickness in Hine's Hole can be influenced by the intensity and proximity of a storm, but this relationship is tenuous given the numerous other factors like translation speed and angle of approach that can impact the local expression of storm intensity. As such, we cannot reliably interpret event bed thickness as a direct proxy of regional scale variability in hurricane intensity.

While hurricanes remain the most likely source of the coarse sediment deposits, we cannot rule out the possibility that locally intense winter storms or tropical storms may produce some of the thinner, less coarse event beds. However, no event beds in the Hine's Hole Composite can be confidently attributed to these types of storms as they remain poorly documented throughout the instrumental record. As demonstrated by Fig. 6d, hurricanes that are: more intense (≥Category 2), more proximal, pass at an angle that subjects Hine's Hole to stronger winds from the front-right or left quadrant (relative to the intensity of the individual storm), and occur after 1940 CE all tend to result in higher confidence attributions. Based on this we have: i. high-confidence that the Hine's Hole Composite archives all ≥Category 2 hurricanes within 75 km provided they are separated by at least 2 years, ii. medium confidence that >Category 1 hurricanes within 75 km or > Category 2 events within 115 km are archived, and iii. Lower confidence that ≤Category 1 hurricanes that pass further than 75 km away are archived (Fig. 6a).

5.3. Changing event frequency

As discussed above, coarse sediment anomalies in the >250 μm data set that exceed the fractional mass threshold of >40.9 mg/cm^3 are almost all coevally timed with proximal passage of hurricanes from 1850 to 2016 CE (Fig. 6). This correlation is also observed for many of the >63 μm anomalies, but there are multiple anomalies in this smaller sediment size-fraction data that do not correspond with any proximal hurricanes in the instrumental record, and may be representative of less intense weather events like tropical storms and anomalously intense winter storms. To facilitate direct comparison to other regional paleohurricane reconstructions, we focus on the >250 μm data for the reconstruction of paleo-storm activity near Hine's Hole as most of these event beds are likely indicative of proximal hurricane intensity storms based on the attribution analysis in section *5.2. Calibrating the record to historical hurricanes*. Specifically, we interpret this record from the liberal counting method as, by nature, sedimentary records of hurricanes represent a minimum-count of hurricane activity over time (Woodruff et al., 2008).

In the 100-yr moving window liberal counts (Fig. 7a), hurricane event bed frequency is above the significance threshold in the oldest portion of the record from 1530 to 1580 CE and 1605–1625 CE, with an average of 22.7 hurricanes/century ±1.7 spanning this ~100 year period from 1530 to 1625 CE. Storm frequency diminished from 1630 to 17,300 CE, with an average of 17.3 hurricanes/century ±2. Following this less active period, event bed frequency reached maximum sustained levels and exceeded the site-specific event-frequency threshold of 21.9 hurricanes/century from 1730 to 1890 CE, with a maximum of 33 hurricanes/century and an average 27.4 hurricanes/century ±3.6. Archived event bed frequency was lowest from 1890 to 1960 CE, with a minimum of 7 hurricanes/century and an average 11.6 hurricanes/century ±4.1.

The 50-year window counts (Fig. 7b), which were doubled to normalize to hurricanes/century, emphasize changes in hurricane frequency that occur at a multidecadal scale. In these counts, two early active intervals are observed from 1505 to 1530 CE (average 27.8 hurricanes/century ±4.3) and from 1570 to 1620 CE (average 28.1 hurricanes/century ±4.2). Event bed frequency from 1505 to 1570 CE and 1620–1710 CE never exceeded the site-specific significance threshold of 21.9 hurricanes/century for sustained periods; however, these two-time windows had an average 15.4 hurricanes/century ±3 which is higher than the average event bed frequency during the instrumental period from 1850 to 2016 CE (14.7 hurricanes/century ±9.6). The longest and most active interval occurred from 1710 to 1875 CE, with an average

28.6 hurricanes/century ±5.7 and a maximum of 40 hurricanes/century. During this 165-year active interval, event bed counts drop to ~19 hurricanes/century from 1730 to 1745 CE before elevating back to above the significance threshold. In the 50-year window counts, activity is lowest from 1905 to 1985 CE, with an average of 8 hurricanes/century ±3.1, which falls just below the site-specific frequency lower significance threshold of 8.5 hurricanes/century.

Overall, the 100-year and 50-year counts are very similar, especially from 1600 to 2016 CE. However, the 100-year window counts fail to capture the multidecadal variability from 1505 to 1620 CE, where the 50-year window counts document two statistically significant active intervals from 1505 to 1530 CE and 1570–1620 CE that are separated by a 40-year lull in activity. Instead, the 100-year window averages these two active periods together with the lull, resulting in a ~ 100-year period from 1530 to 1625 where average storm frequency is 22.7 hurricanes/century ±1.7, which is just above the upper significance threshold of 21.9 hurricanes/century. As such, we suggest that the 50-year window better represents the multi-decadal variability in intense storm frequency that the Hine's Hole Composite is particularly well suited to archive given its high-sedimentation rate that enables clear distinction of multiple event deposits within a relatively short temporal range (1–5 years). The 50-year window counts will therefore be the primary focus of the discussion hereafter.

5.4. Regional hurricane patterns

The evidence from Hine's Hole for significantly higher hurricane activity in the past than what has been observed throughout the ~170 year-long instrumental record has also been documented by other proxy-based and historical reconstructions. Near the Florida Keys, for example, Trouet et al. (2016) inferred that elevated periods of hurricane frequency suppressed growth in south Florida slash pine trees (*Pinus elliottii* var. *densa*, labelled as TC_{supp} in Fig. 8c). It is thought that high-winds and saltwater intrusion from hurricanes causes diminished growth in slash pines, which can be observed from annual tree ring thickness (Trouet et al., 2016). Given the nearly-annual sedimentation rate in Hine's Hole and annual-scale resolution of tree ring growth-based proxies, Hine's Hole and tree ring evidence of hurricane activity are highly comparable. Trouet et al. (2016) demonstrated that on a decadal basis, tree ring growth suppression in slash pines from Big Pine Key (Florida Keys; Fig. 1) correlates well with ≥Category 1 hurricane frequency within ~160 km of Big Pine Key since 1850 CE (TC_{supp}; Fig. 8c). This record was extended to 1495 CE by compiling documentary evidence of 657 Spanish shipwrecks caused by storm activity from 1495 to 1825 CE (abbreviated as TC_{ship} in Fig. 8c), and a historical reconstruction of tropical cyclone activity based on storm observations in Spanish historical documents from the Archivo General de Indias (abbreviated as $TC_{archive}$ in Fig. 8c; García-Herrera et al., 2005). These records show decadal scale similarities to TC_{supp} during the ~110 years of overlap from 1710 to 1820 CE (Fig. 8c).

The Hine's Hole Composite and TC_{ship} (Trouet et al., 2016) each suggest a ~ 20-year significant active period for storm impacts in the Florida Straits from around 1500 CE (AI-1, Fig. 8b, c). After a 30 year lull, Hine's Hole Composite, TC ship, and $TC_{archive}$ (García-Herrera et al., 2005) all suggest a prolonged increase in regional hurricane impact frequency from 1550 to 1620 CE followed by a relatively less active period from 1620 to 1700 CE. Beginning around 1710–1740 CE, Hine's Hole Composite, TC_{supp}, TC_{ship}, and $TC_{archive}$ all suggest a substantial increase in hurricane activity that spans until around 1870 CE, when the Hine's Hole Composite archives the most frequent event beds over the last 530 years (Fig. 8). Beginning around 1860–1880 CE, the Hine's Hole Composite and TC_{supp} both suggest an overall decrease in regional hurricane activity. TC_{supp} does record spikes in hurricane activity from 1920 to 1940 CE, 1960–1970 CE, and 1990–2010 CE that are not detected in the 100-year or 50-year moving window counts of the Hine's Hole Composite. However, based on the attribution of hurricanes to

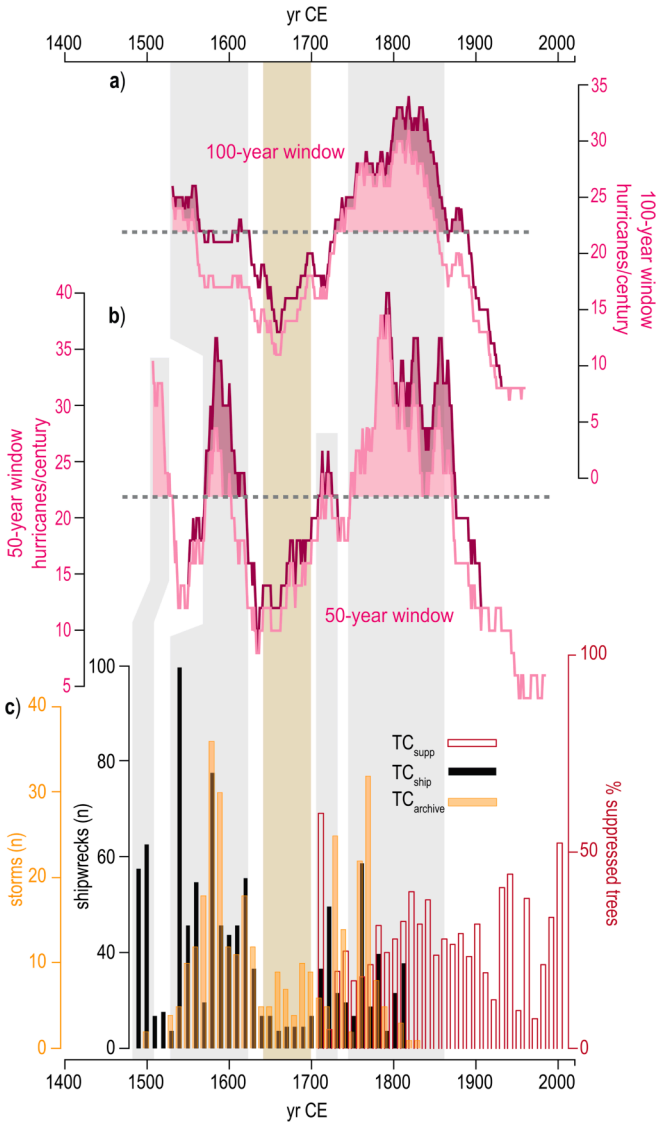

Fig. 8. a) The 100-year and b) 50-year moving window counts of most ≥Category 1 hurricanes/century within 115 km of Hine's Hole on Cay Sal Bank (this study). c) and d) are modified from Fig. 3A, B in Trouet et al. (2016), where TC_{supp} is the percentage of 38 examined south Florida slash pine (*Pinus elliottii* var. *densa*) trees whose rings record a period of suppressed growth related to hurricanes (red bars), TC_{ship} is a compilation of 657 Spanish shipwreck events in the Caribbean from 1495 to 1825 CE (black bars) based on Marx (1987), $TC_{archive}$ is a historical record of Caribbean tropical cyclones compiled from the ship log archives of the Spanish Armada (orange bars; (García-Herrera et al., 2005). Each of the datasets in c) are shown compiled into decadal bins as reported by (Trouet et al., 2016). (For interpretation of the references to colour in this figure legend, the reader is referred to the web version of this article.)

>250 μm coarse sediment anomalies (section *5.2 Calibrating the record to historical hurricanes*), up to 6 hurricanes from 1919 to 1940 CE could leave deposits in Hine's Hole. This suggests that the differences in the records over the last 120 years may be related to variability in the counting resolution of the records coupled with age-model uncertainty rather than spatial variance in hurricane frequency between the Cay Sal Bank and the Florida Keys alone. Winkler et al. (2020) demonstrated that the frequency of proximal ≥Category 2 hurricane passage can vary considerably over the ~200 km stretch from Hine's Hole to Big Pine Key over the last 170 years, so some variance is to be expected between these two records. That said, similarities in the i. timing of active intervals, ii. temporal resolution (near-annual), and iii. Record sensitivity

(≥Category 1 hurricanes within 115–160 km radius) extend across the Hine's Hole Composite, Trouet et al. (2016) compiled records, and the García-Herrera et al. (2005) documentary record lend confidence to the Hine's Hole sedimentary age model. Collectively, these regional records suggest that significant multidecadal- to centennial-scale variations in hurricane frequency are archived over the last 530 years, and that these changes are temporally consistent in the region of Cay Sal Bank and the Florida Keys.

A series of near annually-resolved records of paleo-hurricane activity have been developed from across the eastern portion of the Bahamian Archipelago (Wallace et al., 2019; Wallace et al., 2021b; Wallace et al., 2021c; Winkler et al., 2020) (Figs. 1 and 9). Comparisons must be tempered as the temporal length of the different sedimentary records plotted in Fig. 9 and the individual site sensitivity of the different blue holes they come from is not constant (i.e., their individual potential to record hurricane passage). For example, a ~ 700-year long paleo-hurricane record that records most ≥Category 2 hurricanes within 50 km and most ≥Category 4 hurricanes within 75 km was developed from a the upper 9 m of sediment accumulated in Thatchpoint Blue Hole (Fig. 9a) (Winkler et al., 2020). Thatchpoint Blue Hole is a 70 m deep, 50 m wide blue hole located in a ~ 2 m deep subtidal carbonate lagoon on the western margin of Great Abaco Island. The three blue holes whose sediment archives comprise the 1500 year-long South Andros Stack (Fig. 9b) are found in 0.5–1 m deep tidal inlet channels on the southern tip of Andros Island, and tend to only record ≥Category 3 hurricanes within 50 km (Wallace et al., 2019). The 1050 year Long Island Blue Hole reconstruction is from an 11 m long sediment record collected from a blue hole in a 1–2 m deep subtidal lagoon on the northwest shore of Long Island in the central Bahamas (Fig. 9d). The Long Island Blue Hole record is most likely to record ≥Category 3 hurricane passing within 75 km to the east or north of Long Island or ≥ Category 4 hurricanes passing to the west or south (Wallace et al., 2021c). Finally, Middle Caicos Blue Hole (Fig. 9e) is a 1550 year record derived from a 13.5 m sediment accumulation in a blue hole located in a subtidal lagoon on the western side of Middle Caicos Island that tends to record most ≥Category 2 hurricanes passing within 100 km to the south of the site (Wallace et al., 2021b). Despite the varying levels of consistency in the timing and magnitude of active/inactive intervals of hurricane impacts across these records, some consistent patterns between sites are beginning to emerge that are at times evident in the 530-year long Hine's Hole Composite (Fig. 10b).

The first statistically significant active interval in the Hine's Hole Composite is from 1505 to 1530 CE in the 50-year counts. While this active interval is only recorded for ~25 years at the base of the Hine's Hole Composite, it is unknown how far back in time it may extend. As demonstrated in Fig. 9, it is possible that this active interval coincides with the onset of active periods observed from 1480 to 1510 CE in the 50-year window hurricanes/century counts from Thatchpoint Blue Hole in Abaco (Winkler et al., 2020), 1200–1480 CE in the South Andros Stack from (Wallace et al., 2019; Winkler et al., 2020), and from 1395 to 1500 CE in Long Island Blue Hole (Wallace et al., 2021c). The second active interval in the 50-year window counts from the Hine's Hole Composite from 1570 to 1620 CE occurs during the most prolonged active interval at Thatchpoint Blue Hole (1500–1655 CE), during which time the 50-year window counts from Thatchpoint Blue Hole record up to 16 hurricanes/century from 1525 to 1600 CE. Active intervals archived by Long Island Blue Hole from 1590 to 1650 CE and Middle Caicos Blue Hole (Wallace et al., 2021b) from 1550 to 1655 CE also partially overlap this active interval from Hine's Hole. The South Andros Stack record notably records a lull in activity from ~1500–1600 CE, making it anti-phased with the other near-annually resolved Bahamian records during this time. This spatiotemporal variance suggests that spatial heterogeneity in hurricane frequency throughout The Bahamas from 1850 CE- present observed by Winkler et al. (2020) is likely persistent over longer timescales, and may be caused by inherent stochastic variability in storm tracks that can produce significant centennial-scale hurricane frequency variability in reconstructions from The Bahamas (Wallace et al., 2021a). Notably, all of the near-annually resolved Bahamian records aside from the South Andros Stack observe 50-to-100-year period of diminished hurricane impact frequency during the activity lull from 1605 to 1740 CE in the Hine's Hole Composite and the historical and tree-ring compilations by Trouet et al. (2016) and García-Herrera et al. (2005).

The most prominent active interval in the Hine's Hole Composite extends from 1710 to 1875 CE in the 50-year window counts and from 1730 to 1890 CE in the 100-year window counts. During this 130-year period, brief spikes of increased activity are recorded by Thatchpoint Blue Hole from 1790 to 1810 CE, but hurricanes/century are otherwise relatively low. The tail end of most recent active interval in the South Andros Stack that began around 1600 CE overlaps active interval from 1720 to 1780 CE documented in the Hine's Hole Composite. Finally, both Long Island Blue Hole and Middle Caicos Blue Hole archive heightened hurricane activity from 1775 to 1845 CE and 1675–1910 CE respectively, each overlapping the majority of this Hine's Hole active interval. Aside from Thatchpoint Blue Hole, these records all document relatively low hurricane frequency throughout the instrumental record from 1850 to 2016 CE. Farther to the southeast, a 2000-year long lower-resolution sedimentary reconstruction from Scrub Island in the lesser Antilles records its most active period in hurricane strikes from 1750 to 1850 CE (Biguenet et al., 2021), which also indicates that the 1720–1875 CE period represents an active interval for hurricanes in the Caribbean.

Although the duration of the active intervals is never fully consistent across the five paleo-hurricane records in Fig. 9, most records overlap for some portion of each of the three active intervals archived by the Hine's Hole Composite. The differences in the records is likely related to the variance in each site's recording sensitivity; however, significant spatial gradients exist in the frequency of hurricane impacts across the Bahamian Archipelago throughout the instrumental record (Winkler et al., 2020). For instance, islands like Great Abaco in the northern Bahamas experienced 11–16 ≥ Category 2 hurricanes within 50 km since 1850 CE, whereas areas around Cay Sal Bank, Andros, and Long Island in the central Bahamas had 3 to 4 ≥ Category 2 hurricanes within 50 km during the same time (Fig. 1b).

Analysis of over 50,000 downscaled storms from last-millennium simulations reveal that inherent stochastic variability in storm tracks alone are capable of producing significant centennial scale variability in Caribbean hurricane frequency (Wallace et al., 2021a). Therefore, caution should be exercised when using just one paleoclimate record to interpret broader regional climatic change. Motivated by this, recent studies have developed a 1500 year long near-annually resolved compilation of paleo-hurricane reconstructions from The Bahamas to develop more robust regional signals that increase probability of sampling the full scope of intra-regional spatial variations in storm tracks (Fig. 10b; see Wallace et al., 2021c for detailed compilation methods and Wallace et al., 2021b for most recent data inclusion). This Bahamas Compilation includes all non-duplicate hurricane deposits identified from the individual records included for each island (i.e., a single hurricane that produced event beds at multiple sites on a single island is only counted once), which were then smoothed with a 100-year moving window. The included study sites are plotted in Fig. 1a, and The Bahamas compilation includes all records from Fig. 9 aside from Hine's Hole (Wallace et al., 2019; Wallace et al., 2021b; Wallace et al., 2021c; Winkler et al., 2020).

As seen in Fig. 10a, b, both the 100-year and 50-year moving window hurricanes/century counts archived by the Hine's Hole Composite shows remarkable similarities to the Bahamas Compilation over the last 600 years. Aside from brief lulls in activity from 1530 to 1570 CE and 1730–1745 CE in the 50-year window counts, the Hine's Hole Composite documents significantly higher regional hurricane activity from 1505 to 1620 CE and from 1710 to 1875 CE. These two periods largely overlap with heightened regional hurricane activity in the Bahamas Compilation

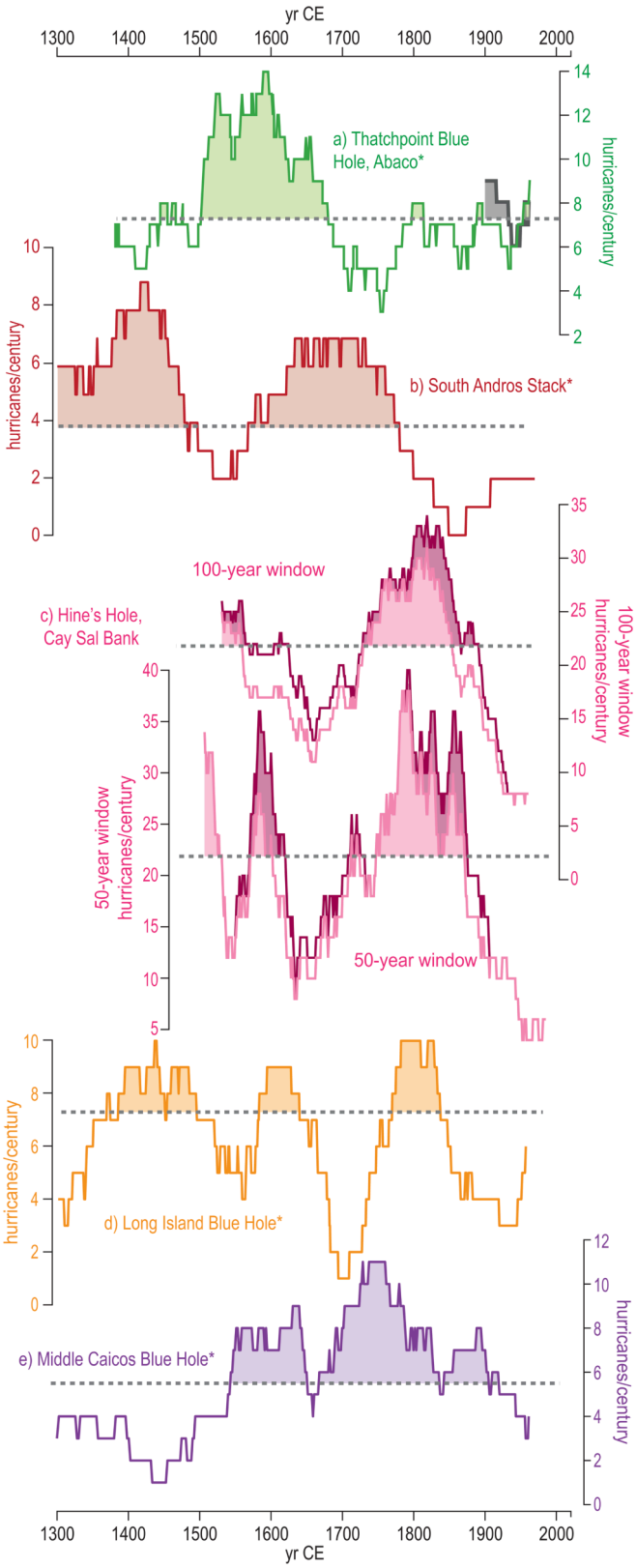

Fig. 9. Hurricanes/century from near annually resolved hurricane reconstructions across the Bahamian Archipelago (see Fig. 1 for site locations). Starting from northernmost locale: a) ≥ Category 2 (3) hurricanes/century within 50 (75) km of Thatchpoint Blue Hole on Abaco Island (Winkler et al., 2020); b) ≥ Category 3 hurricanes/century within 50 km of the Southern Andros region based on the stacked record of three blue hole archives (Wallace et al., 2019; Winkler et al., 2020); c) The 100-year and 50-year moving window counts of most ≥Category 1hurricanes/century within 115 km of Hine's Hole on Cay Sal Bank (this study); d) ≥ Category 2 hurricanes/century within 100 km to the south of Long Island Blue Hole (Wallace et al., 2021c); and e) ≥ Category2 hurricanes/century within 75 km of Middle Caicos Ocean Hole on Middle Caicos (Wallace et al., 2021b). For each reconstruction, the grey dashed line and the colored in portion above it represent the upper significance threshold for hurricane frequency used in each study. (For interpretation of the references to colour in this figure legend, the reader is referred to the web version of this article.)

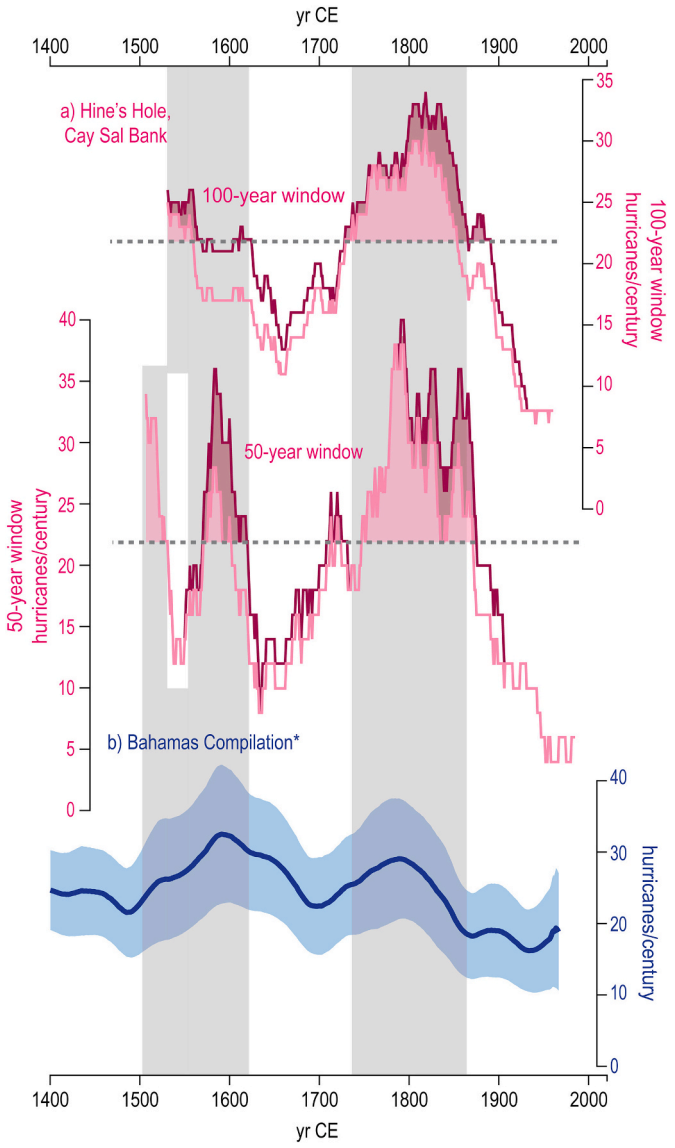

Fig. 10. a) The 100-year and 50-year moving window counts of most ≥Category 1 hurricanes/century within 115 km of Hine's Hole on Cay Sal Bank (this study); b-d) Adapted from Fig. 10 of Wallace et al. (2021b). Compilations of paleo-hurricane records from b) the Bahamian Archipelago which is referred to as the Bahamas Compilation (all studies from Fig. 8 aside from Hine's Hole; blue). The compilation methods are detailed in (Wallace et al., 2021b; Wallace et al., 2021c). The shaded confidence intervals are calculated from the ages produced in Monte Carlo age-simulations run using the Bayesian age modelling program Bacon (Blaauw and Christen, 2011) for each of the contributing records. The compilations shown were smoothed with a 100-year moving window. (For interpretation of the references to colour in this figure legend, the reader is referred to the web version of this article.)

from 1530 to 1625 CE and 1725–1830 CE (Fig. 10b). The large sampling radius and sensitivity of the Hine's Hole Composite allowed it to archive 110 potential hurricane deposits from 1480 to 2016 CE. During this time, the other 4 near-annually resolved Bahamian paleo-hurricane reconstructions collectively archived 128 distinct event beds (average 32 per reconstruction) that were likely deposited by proximal ≥Category 2–3 hurricanes. Both the Hine's Hole Composite and Bahamas Compilation tend to record 10–40 hurricanes/century over the last 600 years. Of the 23 storms that passed within 115 km of Hine's Hole since 1850 CE, 9 formed in the Main Development Region in the Atlantic, 6 formed to the northeast of the Bahamian Archipelago, and 8 formed in the Southern Caribbean (Supplementary Fig. S5), meaning that the storms that are most likely to be archived in the Hine's Hole Composite are evenly distributed between the major regions of Atlantic cyclogenesis throughout the instrumental record. It is therefore possible that the wide variety of storms (i.e., point of origin, strength, track direction) and increased archival rate in the Hine's Hole Composite Record make it an exceptional record for recording broad regional trends in hurricane frequency. Regardless of the mechanisms, the Hine's Hole Composite provides substantial evidence in support of regional hurricane patterns that emerge from recent regional compilations of more intense hurricane strikes across the Bahamian Archipelago. While the geographic area sampled by the Hine's Hole Composite is less than the cumulative scope of the Bahamas Compilation, the higher temporal resolution means it is less likely to undercount hurricanes in consecutive years as other sites in the Bahamas Compilation, but we acknowledge that hurricanes/century may also at times be overcounted in Hine's Hole if certain event beds were actually deposited by other mechanisms (e.g., anomalously intense winter storms). Furthermore, the fact that it is a single-site record means that there is also less chance of overcounting storms that may have been recorded by multiple sites within the Bahamas Compilation.

6. Conclusions

Hine's Hole on Cay Sal Bank archives an exceptionally high-resolution record of high-energy event deposits frequency due to its high sediment accumulation rate. Cay Sal Bank is partially drowned, with an average water depth of ~10 mbsl, meaning that Hine's Hole can be exposed to hurricane wind and waves regardless of passage direction and with minimal effects geomorphologic effects from other coastal and terrestrial systems. Indeed, we observe exceptional temporal correspondence of the 19 > 250 μm coarse sediment anomalies in the Hine's Hole Composite from 1850 to 2016 CE, to the 23 ≥ Category 1 hurricanes within 115 km of Hine's Hole throughout the instrumental record. Based on this modern calibration, we conclude that the Hine's Hole Composite archives sedimentary evidence of most ≥Category 1 hurricanes through the 530-year record,. In total, the Hine's Hole Composite documents 100 (conservative count) to 110 (liberal count) >250 μm coarse sediment anomalies that were most likely deposited by hurricanes from 1480 to 2016 CE, resulting in an average of 18.7 to 20.6 hurricanes/century based on 50-year sliding window counts. Only 20 > 250 μm event beds were recorded from 1850 to 2016 CE, averaging to just ~12 hurricanes/century. However, three periods earlier in the record archive significantly higher levels of hurricane activity from 1505 to 1530 CE (average 27.8 hurricanes/century ±4.3), 1570–1620 CE (average 28.1 hurricanes/century ±4.2), and 1710–1875 CE (28.6 hurricanes/century ±5.7).

This reconstruction demonstrates further that centennial to multi-decadal scale Bahamian hurricane frequency can vary significantly in response to climatic and stochastic forcing within the pre-industrial climate system (Wallace et al., 2019; Wallace et al., 2021a; Wallace et al., 2021b; Wallace et al., 2021c; Winkler et al., 2020). The most active century from 1770 to 1870 CE documents 34 storm event beds, compared to just 8 event beds during the least active century from 1916 to 2016 CE. This demonstrates that recurrence intervals based on the ~170-year instrumental record alone can severely underestimate the threat hurricanes pose certain localities. We emphasize that median-age estimates for the onset and offset of active intervals as well as the temporal extent of the record all have an average uncertainty of ±35 years, with an additional ±20 years related ΔR correction uncertainties (Supplemental 4). However, these active periods are synchronous with frequent hurricane impacts documented by a high-resolution tree ring reconstruction in the Florida Keys (Trouet et al., 2016). The Hine's Hole Composite record further documents the substantial intra-island spatial heterogeneity in hurricane frequency across the Bahamian Archipelago that is observed in instrumental and paleo-hurricane records (Wallace et al., 2019; Wallace et al., 2021b; Wallace et al., 2021c; Winkler et al.,

2020). However, hurricanes/century derived from the 50-yr counts of the Hine's Hole Composite show strong correspondence with a regional compilation of 4 near-annually resolved reconstructions from across the Bahamian Archipelago (Wallace et al., 2021b; Wallace et al., 2021c), particularly with regard to decreasing hurricane frequency from 1650 to 1740 CE and from 1850 CE to present, and heightened frequency from 1530 to 1625 CE and 1–1830 CE. Given that only 18 m of the ≥60 m of accumulation in Hine's Hole is presented here, this site offers unprecedented potential for developing a near-annually resolved record of multidecadal hurricane frequency variability throughout the last 2000 years.

Data availability

All conventional radiocarbon dates can be found in Supplementary Table S2, and the remaining sedimentological and reconstruction data are available on the National Climatic Data Center (https://www.ncdc.noaa.gov/paleo/study/34252).

Declaration of Competing Interest

The authors declare that they have no known competing financial interests or personal relationships that could have appeared to influence the work reported in this paper.

Acknowledgements

This work was funded by the Dalio Explore Foundation (to JPD and PJvH.), National Science Foundation Awards OCE-1356509, OCE-1356708, OCE-1854917, OCE-1903616, and ICER-1854980 (to JPD and PJvH.), Geological Society of America Student Research Grant (to TSW), Texas Sea Grant: Grant in Aid of Graduate Research (to T.S.W), Sigma Xi Grant in Aid of Graduate Research (to TSW), and the Texas A&M University at Galveston Boost Scholarship (to TSW).

Field and technical support was provided by Victoria Keeton and Stephanie Madsen, Stuart McLoughlin (Science Officer) and the rest of crew of the M/V Alucia, the RV Kate, and the RV Endsley. Additional laboratory support was provided by NSF Research Experience for Undergraduates fellow Sarah Swierz, along with Texas A&M University at Galveston undergraduate research interns Meghan Horgan, Kate Bricken, Laura Hurt, Jamie Lilly Garland, and Olivia Shipley.

We thank the Khaled bin Sultan Living Ocean Foundation for sharing habitat and bathymetric data used to produce Fig. 2a. We also thank our reviewers, including Dr. Samuel Purkis, Dr. Pierre Sabatier, and one other anonymous reviewer for their constructive comments and valuable insight that helped improve this manuscript.

References

Arcos, N., Chacon-Barrantes, S., Varner, J., Lopez, A., 2018. Caribbean and Adjacent Regions Tsunami Sources and Models (CATSAM) Map Viewer.
Ashmore, S., Leatherman, S.P., 1984. Holocene sedimentation in Port Royal Bay, Bermuda. Mar. Geol. 56, 289–298.
Barkan, R., Uri, S., Lin, J., 2009. Far field tsunami simulations of the 1755 Lisbon earthquake: Implications for tsunami hazard to the US East Coast and the Caribbean. Mar. Geol. 264, 109–122.
Biguenet, M., Sabatier, P., Chaumillon, E., Chagué, C., Arnaud, F., Jorissen, F., Coulombier, T., Geba, E., Cordrie, L., Vacher, P., 2021. A 1600 year-long sedimentary record of tsunamis and hurricanes in the Lesser Antilles (Scrub Island, Anguilla). Sediment. Geol. 412, 105806.
Blaauw, M., Christen, A., 2011. Flexible paleoclimate age-depth models using an autoregressive gamma process. Bayesian Anal. 6, 457–474.
Brandon, C.M., Woodruff, J.D., Lane, P., Donnelly, J.P., 2013. Constraining flooding conditions for prehistoric hurricanes from resultant deposits preserved in Florida sinkholes. Geochem. Geophys. Geosyst. 14, 2993–3008.
Bregy, J.C., Wallace, D.J., Minzoni, R.T., Cruz, V.J., 2018. 2500-year paleotempestological record of intense storms for the northern Gulf of Mexico, United States. Mar. Geol. 396, 26–42.
Broecker, W.S., Olson, E.A., 1961. Lamont radiocarbon measurements VIII. Radiocarbon 3, 176–204.
Chavas, D.R., Lin, N., Dong, W., Lin, Y., 2016. Observed tropical cyclone size revisited. J. Clim. 29, 2923–2939.
Chenoweth, M., Divine, D., 2008. A document-based 318-year record of tropical cyclones in the Lesser Antilles, 1690–2007. Geochem. Geophys. Geosyst. 9.
Davenport, F.V., Burke, M., Diffenbaugh, N.S., 2021. Contribution of historical precipitation change to US flood damages. Proc. Natl. Acad. Sci. 118.
Denomee, K.C., Bentley, S.J., Droxler, A.W., 2014. Climatic control on hurricane patterns: a 1200-y near-annual record from Lighthouse Reef, Belize. Sci. Rep. 4, 7.
Diaz, M., Macario, K., Gomes, P., Álvarez-Lajonchere, L., Aguilera, O., Alves, E., 2017. Radiocarbon marine reservoir effect on the northwestern coast of Cuba. Radiocarbon 59, 333.
DiNapoli, R.J., Fitzpatrick, S.M., Napolitano, M.F., Rick, T.C., Stone, J.H., Jew, N.P., 2021. Marine reservoir corrections for the Caribbean demonstrate high intra-and inter-island variability in local reservoir offsets. Quat. Geochronol. 61, 101126.
Donnelly, J.P., Woodruff, J.D., 2007. Intense hurricane activity over the past 5,000 years controlled by El Niño and the West African Monsoon. Nature 447, 465–468.
Donnelly, J.P., Hawkes, A.D., Lane, P., MacDonald, D., Shuman, B.N., Toomey, M.R., van Hengstum, P.J., Woodruff, J.D., 2015. Climate forcing of unprecedented intense-hurricane activity in the last 2000 years. Earth Future 3, 49–65.
Druffel, E.R., 1997. Pulses of rapid ventilation in the North Atlantic surface ocean during the past century. Science 275, 1454–1457.
Druffel, E.M., Linick, T.W., 1978. Radiocarbon in annual coral rings of Florida. Geophys. Res. Lett. 5, 913–916.
Emanuel, K.A., 2013. Downscaling CMIP5 climate models shows increased tropical cyclone activity over the 21st century. Proc. Natl. Acad. Sci. U. S. A. 110, 12219–12224.
Emanuel, K., Sundararajan, R., Williams, J., 2008. Hurricanes and global warming: results from downscaling IPCC AR4 simulations. Bull. Am. Meterorol. Soc. 89, 347–367.
García-Herrera, R., Gimeno, L., Ribera, P., Hernández, E., 2005. New records of Atlantic hurricanes from Spanish documentary sources. J. Geophys. Res. 110, 1–7.
Gischler, E., Shinn, E.A., Oschmann, W., Fiebig, J., Buster, N.A., 2008. A 1500-year Holocene Caribbean climate archive from the Blue Hole, Lighthouse Reef, Belize. J. Coast. Res. 24, 1495–1505.
Goldberg, W.M., 1983. Cay Sal Bank, Bahamas: a biologically impoverished, physically controlled environment. Atoll Res. Bull. 271, 1–17.
Hadden, C.S., Schwadron, M., 2019. Marine reservoir effects in eastern oyster (Crassostrea virginica) from southwestern Florida, USA. Radiocarbon 61, 1501–1510.
Heaton, T.J., Köhler, P., Butzin, M., Bard, E., Reimer, R.W., Austin, W.E., Ramsey, C.B., Grootes, P.M., Hughen, K.A., Kromer, B., 2020. Marine20—the marine radiocarbon age calibration curve (0–55,000 cal BP). Radiocarbon 1–42.
Hine, A.C., Steinmetz, J.C., 1984. Cal Sal Bank, Bahamas: a partially drowned carbonate platform. Mar. Geol. 59, 135–164.
Khan, N.S., Ashe, E., Horton, B.P., Dutton, A., Kopp, R.E., Brocard, G., Engelhart, S.E., Hill, D.F., Peltier, W., Vane, C.H., 2017. Drivers of Holocene sea-level change in the Caribbean. Quat. Sci. Rev. 155, 13–36.
Knapp, K.R., Kruk, M.C., Levinson, D.H., Diamond, H.J., Neumann, C.J., 2010. The international best track archive for climate stewardship (IBTrACS) unifying tropical cyclone data. Bull. Am. Meteorol. Soc. 91, 363–376.
Knapp, K.R., Diamond, H.J., Kossin, J.P., Kruk, M.C., Schreck III, C.J., 2018. International Best Track Archive for Climate Stewardship (IBTrACS) Project, Version 4. [Atlantic Basin US_SSHS subset]. NOAA National Centers for Environmental Information. https://data.nodc.noaa.gov/cgi-bin/iso?id=gov.noaa.ncdc:C01552 (Accessed 24 Jan 2020).
Knutson, T., Camargo, S.J., Chan, J.C., Emanuel, K., Ho, C.-H., Kossin, J., Mohapatra, M., Satoh, M., Sugi, M., Walsh, K., 2020. Tropical cyclones and climate change assessment: Part II. Projected response to anthropogenic warming. Bull. Am. Meteorol. Soc. 101 (3), E303–E322.
Kondo, Y., 1987. 847. Burrowing depth of infaunal bivalves: observation of living species and its relation to shell morphology. In: Transactions and Proceedings of the Paleontological Society of Japan. New Series. Palaeontological Society of Japan, pp. 306–323.
Korty, R.L., Emanuel, K.A., Huber, M., Zamora, R.A., 2017. Tropical cyclones downscaled from simulations with very high carbon dioxide levels. J. Clim. 30, 649–667.
Kossin, J.P., 2018. A global slowdown of tropical-cyclone translation speed. Nature 558, 104–107.
Kourafalou, V.H., Kang, H., 2012. Florida current meandering and evolution of cyclonic eddies along the Florida Keys Reef Tract: are they interconnected? J. Geophys. Res. 117.
Landsea, C.W., Harper, B.A., Hoarau, K., Knaff, J.A., 2006. Can we detect trends in extreme tropical cyclones? Science 313, 452–454.
Lane, P., Donnelly, J.P., Woodruff, J.D., Hawkes, A.D., 2011. A decadally-resolved paleohurricane record archived in the late Holocene sediments of a Florida sinkhole. Mar. Geol. 287, 14–30.
Lighty, R.G., Macintyre, I.G., Stuckenrath, R., 1982. Acropora palmata reef framework: a reliable indicator of sea level in the western Atlantic for the past 10,000 years. Coral Reefs 1, 125–130.
Lin, Y., Zhao, M., Zhang, M., 2015. Tropical cyclone rainfall area controlled by relative sea surface temperature. Nat. Commun. 6, 6591.
Liu, K.-B., Fearn, M.L., 1993. Lake-sediment record of late Holocene hurricane activities from coastal Alabama. Geology 21, 793–796.
Liu, K., Fearn, M.L., 2000. Reconstruction of prehistoric landfall frequencies of catastrophic hurricanes in NW Florida from lake sediment records. Quat. Res. 52, 238–245.

Mallinson, D.J., Smith, C.W., Mahan, S., Culver, S.J., McDowell, K., 2011. Barrier island response to late Holocene climate events, North Carolina, USA. Quat. Res. 76, 46–57.
Marx, R.F., 1987. Shipwrecks in the Americas. Courier Corporation.
McAdie, C., Landsea, C., Neumann, C.J., David, J.E., Blake, E.S., 2009. Tropical Cyclones of the North Atlantic Ocean, 1851–2006: With 2007 and 2008 Track Maps Included. US Department of Commerce, National Oceanic and Atmospheric Administration.
Miller, K.G., Kopp, R.E., Horton, B.P., Browning, J.V., Kemp, A.C., 2013. A geological perspective on sea-level rise and its impacts along the US mid-Atlantic coast. Earth Future 1, 3–18.
Oliva, F., Peros, M., Viau, A., Reinhardt, E., Nixon, F., Morin, A., 2018. A multi-proxy reconstruction of tropical cyclone variability during the past 800 years from Robinson Lake, Nova Scotia, Canada. Mar. Geol. 406, 84–97.
Oppenheimer, M., Hinkel, J., 2019. Sea Level Rise and Implications for Low Lying Islands, Coasts and Communities Supplementary Material. IPCC Special Report on the Ocean and Cryosphere in a Changing Climate.
Parsons, T., Geist, E.L., 2008. Tsunami Probability in the Caribbean region, Tsunami Science Four Years after the 2004 Indian Ocean Tsunami. Springer, pp. 2089–2116.
Patricola, C.M., Wehner, M.F., 2018. Anthropogenic influences on major tropical cyclone events. Nature 563, 339–346.
Pielke Jr., R.A., Gratz, J., Landsea, C.W., Collins, D., Saunders, M.A., Musulin, R., 2008. Normalized hurricane damage in the United States: 1900–2005. Nat. Hazards Rev. 9, 29–42.
Purkis, S., Kerr, J., Dempsey, A., Calhoun, A., Metsamaa, L., Riegl, B., Kourafalou, V., Bruckner, A., Renaud, P., 2014. Large-scale carbonate platform development of Cay Sal Bank, Bahamas, and implications for associated reef geomorphology. Geomorphology 222, 25–38.
Purkis, S., Cavalcante, G., Rohtla, L., Oehlert, A.M., Harris, P., Swart, P.K., 2017. Hydrodynamic control of whitings on Great Bahama Bank. Geology 45, 939–942.
Rasmussen, K.A., Haddad, R.I., Neumann, A.C., 1990. Stable-isotope record of organic carbon from an evolving carbonate banktop, Bight of Abaco, Bahamas. Geology 18, 790–794.
Reimer, P.J., Brown, T.A., Reimer, R.W., 2004. Discussion: reporting and calibration of post-bomb 14C data. Radiocarbon 46, 1299–1304.
Reimer, P.J., Austin, W.E., Bard, E., Bayliss, A., Blackwell, P.G., Ramsey, C.B., Butzin, M., Cheng, H., Edwards, R.L., Friedrich, M., Grootes, P.M., Guilderson, T.P., Hajdas, I., Heaton, T.J., Hogg, A.G., Hughen, K.A., Kromer, B., Manning, S.W., Muscheler, R., Palmer, J.G., Pearson, C., van der Plicht, J., Reimer, R.W., Richards, D.A., Scott, E. M., Southon, J.R., Turney, C.S.M., Wacker, L., Adolphi, F., Büntgen, U., Capano, M., Fahrni, S.M., Fogtmann-Schulz, A., Friedrich, R., Köhler, P., Kudsk, S., Miyake, F., Olsen, J., Reinig, F., Sakamoto, M., Sookdeo, A., Talamo, S., 2020. The IntCal20 Northern Hemisphere radiocarbon age calibration curve (0–55 cal kBP). Radiocarbon 62, 725–757.
Sabatier, P., Wilhelm, B., Gentile, F.F., Moiroux, G., Poulenard, J., Develle, A.-L., Bichet, A., Chen, W., Pignol, C., Reyss, J.L., 2017. Timescale-Dependent Interplays of Solar and Temperature Forcing to Explain 6kyrs of Flood Frequency and Intensity in the Western Mediterranean Alps, 5th PAGES Open Science Meeting.
Schmitt, D., Gischler, E., Anselmetti, F.S., Vogel, H., 2020. Caribbean cyclone activity: an annually-resolved Common Era record. Sci. Rep. 10, 1–17.
Smith, A.B., 2020. In: Information, N.N.C.f.E (Ed.), U.S. Billion-dollar Weather and Climate Disasters, 1980 - Present.
Sobel, A.H., Camargo, S.J., Hall, T.M., Lee, C.-Y., Tippett, M.K., Wing, A.A., 2016. Human influence on tropical cyclone intensity. Science 353, 242–246.
Toth, L.T., Cheng, H., Edwards, R.L., Ashe, E., Richey, J.N., 2017. Millennial-scale variability in the local radiocarbon reservoir age of south Florida during the Holocene. Quat. Geochronol. 42, 130–143.
Trouet, V., Harley, G.L., Domínguez-Delmás, M., 2016. Shipwreck rates reveal Caribbean tropical cyclone response to past radiative forcing. Proc. Natl. Acad. Sci. 113, 3169–3174.
Tukey, J.W., 1977. Exploratory Data Analysis. Addison-Wesley Pub. Co., Reading, MA, USA.
Ulm, K., 1990. Simple method to calculate the confidence interval of a standardized mortality ratio (SMR). Am. J. Epidemiol. 131, 373–375.
Vacchi, M., Engelhart, S.E., Nikitina, D., Ashe, E.L., Peltier, W.R., Roy, K., Kopp, R.E., Horton, B.P., 2018. Postglacial relative sea-level histories along the eastern Canadian coastline. Quat. Sci. Rev. 201, 124–146.
van Hengstum, P.J., Donnelly, J.P., Fall, P.L., Toomey, M.R., Albury, N.A., Kakuk, B., 2016. The intertropical convergence zone modulates intense hurricane strikes on the western North Atlantic margin. Sci. Rep. 6 (1), 1–10.
Vecchi, G.A., Knutson, T.R., 2011. Estimating annual numbers of Atlantic hurricanes missing from the HURDAT database (1878–1965) using ship track density. J. Clim. 24, 1736–1746.
Wallace, E., Donnelly, J., van Hengstum, P., Wiman, C., Sullivan, R., Winkler, T., d'Entremont, N., Toomey, M., Albury, N., 2019. Intense hurricane activity over the past 1500 years at South Andros Island, The Bahamas. Paleoceanogr. Paleoclimatol. 34 (11), 1761–1783.
Wallace, E.J., Coats, S., Emanuel, K., Donnelly, J.P., 2021a. Centennial-scale shifts in storm frequency captured in paleohurricane records from The Bahamas arise predominantly from random variability. Geophys. Res. Lett. 48 (e2020GL091145).
Wallace, E.J., Donnelly, J.P., van Hengstum, P.J., Winkler, T.S., Dizon, C., LaBella, A., Lopez, I., d'Entremont, N.E., Sullivan, R.M., Woodruff, J.D., Hawkes, A.D., Maio, C., 2021b. Regional shifts in paleohurricane activity over the last 1500 years derived from blue hole sediments offshore of Middle Caicos Island. Quat. Sci. Rev. 268, 107126.
Wallace, E.J., Donnelly, J.P., van Hengstum, P.J., Winkler, T.S., McKeon, K., MacDonald, D., d'Entremont, N.E., Sullivan, R.M., Woodruff, J.D., Hawkes, A.D., Maio, C., 2021c. 1050 years of hurricane strikes on Long Island in the Bahamas. Paleoceanogr. Paleoclimatol. 36 (e2020PA004156).
Walsh, K.J., Camargo, S.J., Vecchi, G.A., Daloz, A.S., Elsner, J., Emanuel, K., Horn, M., Lim, Y.-K., Roberts, M., Patricola, C., 2015. Hurricanes and climate: the US CLIVAR working group on hurricanes. Bull. Am. Meteorol. Soc. 96, 997–1017.
Walsh, K.J., McBride, J.L., Klotzbach, P.J., Balachandran, S., Camargo, S.J., Holland, G., Knutson, T.R., Kossin, J.P., Lee, T.c., Sobel, A., 2016. Tropical cyclones and climate change. Wiley Interdiscip. Rev. Clim. Chang. 7, 65–89.
Wilhelm, B., Sabatier, P., Arnaud, F., 2015. Is a regional flood signal reproducible from lake sediments? Sedimentology 62, 1103–1117.
Winkler, T.S., van Hengstum, P.J., Donnelly, J.P., Wallace, E.J., Sullivan, R.M., MacDonald, D., Albury, N.A., 2020. Revising evidence of hurricane strikes on Abaco Island (The Bahamas) over the last 700 years. Sci. Rep. 10, 1–17.
Wong, P.P., Losada, I.J., Gattuso, J., Hinkel, J., Khattabi, A., McInnes, K., Saito, Y., Sallenger, A., 2014. Coastal systems and low-lying areas. Climate Change 361–409.
Woodruff, J.D., Donnelly, J.P., Emanuel, K., Lane, P., 2008. Assessing sedimentary records of paleohurricane activity using modeled hurricane climatology. Geochem. Geophys. Geosyst. 9 (9), 1–12.
Woodruff, J.D., Irish, J.L., Camargo, S.J., 2013. Coastal flooding by tropical cyclones and sea-level rise. Nature 504, 44.
Yang, Y., Maselli, V., Normandeau, A., Piper, D.J., Li, M.Z., Campbell, D.C., Gregory, T., Gao, S., 2020. Latitudinal response of storm activity to abrupt climate change during the last 6,500 years. Geophys. Res. Lett. 47 (e2020GL089859).